Archives of Biochemistry and Biophysics 736 (2023) 109538

Contents lists available at ScienceDirect

Archives of Biochemistry and Biophysics

journal homepage: www.elsevier.com/locate/yabbi

Folding of the nascent polypeptide chain of a histidine phosphocarrier protein *in vitro*

José L. Neira [a,b,*], Martina Palomino-Schätzlein [c]

[a] IDIBE, Universidad Miguel Hernández, 03202, Elche, Alicante, Spain
[b] Instituto de Biocomputación y Física de Sistemas Complejos (BIFI), Joint Units IQFR-CSIC-BIFI and GBsC-CSIC-BIFI, Universidad de Zaragoza, 50018, Zaragoza, Spain
[c] ProtoQSAR SL, CEEI-Valencia, Parque Tecnológico de Valencia, Av. Benjamin Franklin 12 (Dep. 8), 46980, Paterna, Valencia, Spain

ARTICLE INFO

Keywords:
Binding
Circular dichroism
Fluorescence
Nascent chain
NMR
Protein-protein interactions

ABSTRACT

The phosphotransferase system (PTS), a metabolic pathway formed by five proteins, modulates the use of sugars in bacteria. The second protein in the chain is the histidine phosphocarrier, HPr, with the binding site at His15. The HPr kinase/phosphorylase (HPrK/P), involved in the bacterial use of carbon sources, phosphorylates HPr at Ser46, and it binds at its binding site. The regulator of sigma D protein (Rsd) also binds to HPr at His15. We have designed fragments of HPr, growing from its N-terminus and containing the His15. In this work, we obtained three fragments, HPr38, HPr58 and HPr70, comprising the first thirty-eight, fifty-eight and seventy residues of HPr, respectively. All fragments were mainly disordered, with evidence of a weak native-like, helical population around the binding site, as shown by fluorescence, far-ultraviolet circular dichroism, size exclusion chromatography and nuclear magnetic resonance. Although HPr38, HPr58 and HPr70 were disordered, they could bind to: (i) the N-terminal domain of first protein of the PTS, EIN; (ii) Rsd; and, (iii) HPrK/P, as shown by fluorescence and biolayer interferometry (BLI). The association constants for each protein to any of the fragments were in the low micromolar range, within the same range than those measured in the binding of HPr to each protein. Then, although acquisition of stable, native-like secondary and tertiary structures occurred at the last residues of the polypeptide, the ability to bind protein partners happened much earlier in the growing chain. Binding was related to the presence of the native-like structure around His15.

1. Introduction

Proteins are synthesized by growing from their N terminus *in vivo*. The co-translational folding of the nascent polypeptide chains is key to maintain a fully operational proteome in cells [1–4]. Specific chaperones bind to the nascent chains after they emerge from the peptide exit tunnel (PET) on the 60S ribosomal subunit to facilitate their *de novo* folding [4,5]. These accessory proteins ensure an effective folding and prevent off-pathway reactions, such as aggregation or unspecific local protein-protein interactions (PPIs) of the ribosome itself, or other components of the translation machinery, with the nascent chain. The studies of the chaperone complexes with the nascent chain have blossomed with the recent use of cryo-electron microscopy [4 and references therein], but the experimental strategies to detect the emergence of elements of native-like protein structure during the polypeptide synthesis on the ribosome, are still scarce. For instance, few details are known about how the isolated nascent chain is folded, if it is, during its release from the PET. Furthermore, it is unknown whether recognizable elements of native secondary structure form early in synthesis, and if various are formed, whether they assemble in a hierarchical, native-like manner. An approach trying to provide answers to the raised questions is to study the nascent polypeptide chain *in vitro* under controlled conditions, i.e., at equilibrium, in the absence of any chaperone and in isolation from the rest of the components within the cell.

In response to environmental variations, bacteria adapt their metabolism by turning on/off the expression of genes [6,7]. One of these metabolic pathways is the bacterial phosphoenolpyruvate (PEP):sugar-dependent, the so-called PEP-dependent phosphotransferase system (PTS), which regulates the use of carbon sources. PTS intervenes in the uptake and transport of several sugars through the cell wall [7,8]. Furthermore, it is also involved in: (i) bacterial movement towards carbon sources (chemotaxis); (ii) nitrogen metabolism; and (iii) other metabolic pathways [7–9]. PTS is formed by phosphoryl-transfer steps from PEP, occurring through several proteins, and involving phosphorylation, for some of them, at histidine residues. The first two

* Corresponding author. IDIBE, Universidad Miguel Hernández, Avda. del Ferrocarril s/n, 03202, Elche, Alicante, Spain.
E-mail address: jlneira@umh.es (J.L. Neira).

https://doi.org/10.1016/j.abb.2023.109538
Received 19 December 2022; Received in revised form 28 January 2023; Accepted 1 February 2023
Available online 3 February 2023

Abbreviations

ANS	8-anilinonaphthalene,1-sulfonate
BLI	biolayer interferometry
DHFR	dihydrofolate reductase
HPrK/P	HPr kinase/phosphorylase
HPrK/P^{bs}	the HPrK/P from *Bacillus subtilis*
CD	circular dichroism
CI2	chymotrypsin inhibitor 2
DOSY	diffusion ordered spectroscopy
EI	enzyme I
EI^{sc}	EI from *Streptomyces coelicolor*
EIN	the N-terminal domain of EI, containing its active site
EIN^{sc}	the EIN from *S. coelicolor*
GdmCl	guanidinium hydrochloride
HPr	histidine-phosphocarrier protein
HPr^{ec}	HPr from Escherichia coli
HPr^{sc}	the full-length, ninety-three residue-long HPr from *S. coelicolor*
HPr$^{9-30}$	fragment comprising residues Gly9-Ala30 of the intact HPr^{sc}
HPr38	fragment derived from HPr^{sc} consisting of the first thirty-eight N-terminal residues of the intact protein
HPr48	fragment derived from HPr^{sc} containing the first forty-eight N-terminal residues of the intact protein
HPr58	fragment derived from HPr^{sc} containing the first fifty-eight N-terminal residues of the intact protein
HPr70	fragment derived from HPr^{sc} containing the first seventy N-terminal residues of the intact protein
ITC	isothermal titration calorimetry
NMR	nuclear magnetic resonance
LB	Luria-Bertani
PEP	phosphoenolpyruvate
PET	peptide exit tunnel
PPI	protein-protein interaction
PTS	PEP-dependent phosphotransferase system
Rsd	regulator of sigma D
Rsd^{ec}	the Rsd from *Escherichia coli*
RU	resonance units in BLI experiments
SDS-PAGE	polyacrylamide gel electrophoresis in the presence of sodium dodecyl sulfate
SEC	size exclusion chromatography
TFE	2,2,2-trifluoroethanol
TSP	3-(Trimethylsilyl)propionic-2,2,3,3-d$_4$ acid
UV	ultraviolet.

proteins in the cascade are common to all PTS substrates: the 64-kDa dimeric phosphocarrier enzyme I (EI), which is phosphorylated by PEP at a histidine; and the monomeric histidine phosphocarrier (HPr), which is phosphorylated by EI at another histidine. The target proteins of HPr are signal transductors, catabolic enzymes, transporters, and in many cases, transcriptional regulators [8–11]. The proteolytic cleavage of EI from *Escherichia coli* yields two domains [12], although these domains are also present in other EI species [12–16]. The N-terminal domain of EI (EIN) comprises, roughly, the first 230 residues of the intact EI: it contains the HPr-binding domain and the active-site histidine [16,17].

In Gram-positive bacteria, HPr has two phosphorylation sites. The PEP-dependent phosphorylation of HPr occurs through EI, being His15 of HPr phosphorylated, and the final receptor is a sugar. In addition, HPr is subjected to regulatory, ATP-dependent phosphorylation at Ser46 by the HPr kinase/phophorylase (HPrK/P) [8,9,11]. We have recently characterized the conformational and biophysical features of the isolated HPrK/P from *Bacillus subtilis*, HPrK/P^{bs} [18], and we have shown that it binds to intact HPr from *Streptomyces coelicolor*, HPr^{sc} [19].

Bacteria also respond to changes by modulation of their transcription machinery. Transcription in bacteria is carried out by a single multi-subunit RNA polymerase. This protein interacts with the σ factors, having a specific promoter recognition activity [20,21]. Bacteria have several σ factors; for instance, *E. coli* encodes seven factors: the primary σ^{70} factor and other six required for the transcription of more specialized genes [22,23]. The anti-σ factor of σ^{70} is a 158-residue-long protein, Rsd (regulator of sigma D), that prevents the transcription of σ^{70}-dependent promoters [24,25]. It has been shown that the de-phosphorylated form of HPr in *E. coli* binds tightly to Rsd through its binding-site histidine, inhibiting the complex formation between Rsd and σ^{70} [26,27]. We have recently shown that the Rsd from *E. coli*, Rsd^{ec}, binds the HPr from *Streptomyces coelicolor* [28]. In *S. coelicolor*, there are as many as 65 σ factors and the interaction of any of their anti-σ factors with HPr^{sc} has not yet been identified [29].

Streptomyces is an actinomycete, Gram-positive organism with high G + C content that grows on a variety of carbon sources. We have carried out a description of the conformational stability and the interactions of HPr^{sc} with EI, EI^{sc} [14,15,30–32], and the EIN^{sc} domain [13,33]; as well as the interactions among the phosphorylated species of both proteins [33]. Based upon these findings, we have designed short peptides interfering with the EIN^{sc} and HPr^{sc} interaction, and exhibiting anti-bacterial activity [32,34]. We have also shown that the fragment containing the first forty-eight residues of HPr^{sc}, HPr48, is mainly disordered and it binds to EIN^{sc}, Rsd^{ec} and HPrK/P^{bs} [19], and, most importantly, it enhances the anti-bacterial properties of several antibiotics.

In this work, we obtained fragments of increasing size from the N terminus of HPr^{sc} by using a combination of protein engineering and chemical cleavage. We isolated and characterized the fragments of HPr^{sc} growing from its N terminus: HPr38 (containing the first thirty-eight residues and similarly for the other fragments in this work), HPr58 and HPr70. All of them contain the binding site His15, and except HPr38, they also have the regulation serine (Ser46), that can be phosphorylated by HPrK/P. The fragments were mainly disordered, as shown by fluorescence, far-ultraviolet (UV) circular dichroism (CD), nuclear magnetic resonance (NMR) and size exclusion chromatography (SEC), although there was a small population of native-like, helical structure around the binding site. These results indicate that the growth of structure in the nascent polypeptide chain of HPr^{sc} was highly cooperative and it did not result from the hierarchical accretion of residual, well-formed secondary structures at each of the different elongating steps. We further measured the affinities of HPr38, HPr58 and HPr70 for EIN^{sc}, HPrK/P^{bs} and Rsd^{ec}, which were within the same order of magnitude of those measured for the corresponding binding reactions of the intact HPr^{sc} with such proteins [19,28,32,33]. Thus, although the acquisition of native-like structure did not occur until the polypeptide chain contained most of the protein residues, binding to the partners already happened at the early stages of the growing HPr^{sc} chain, and it seemed to be related to the presence of the weak, native-like, helical population around its binding site.

2. Materials and methods

2.1. Materials

Ampicillin and isopropyl-β-D-1-thiogalactopyranoside were obtained from Apollo Scientific (Stockport, UK). Imidazole, Trizma base, DNAse, cyanogen bromide, SIGMAFAST protease tablets, Luria-Bertani (LB)

bacterial culture broth, 3-(Trimethylsilyl)propionic-2,2,3,3-d_4 acid (TSP) and His-Select HF nickel resin were purchased from Sigma-Aldrich (Madrid, Spain). Amicon centrifugal devices with a cut-off molecular weight of 3 kDa were from Millipore (Barcelona, Spain). Dialysis tubing with a molecular weight cut-off of 3.5 kDa was from Spectrapore (VWR, Barcelona, Spain). High-purity oligonucleotides for site-directed mutagenesis were synthesized by Invitrogen (Barcelona, Spain). Thrombin was from GE Healthcare (Barcelona, Spain). The rest of the used materials were of analytical grade. Water was deionized and purified on a Millipore system.

2.2. Expression and purification of HPr^{sc} fragments

The peptide containing residues 9 to 30 of the intact HPr, HPr$^{9\text{-}30}$, was obtained from NZYTech (Lisbon, Portugal) by using chemical synthesis, with purity higher than 95% as tested by mass spectra, as described [35].

The HPr^{sc} vector, with a His_6-tag at its N-terminus, was a kind gift from Prof. Fritz Titgemeyer (Erlangen, Germany). The wild-type, full-length HPr^{sc} comprises residues from 1 to 93. This construction has a natural methionine at position 48, and another one where the protein is fused to the His_6-tag at its N terminus (Met1), resulting from cloning in the pET15b vector. However, to proceed with a chemical BrCN cleavage in designed mutants, we must remove it, as well as Met48.

We designed a mutant of HPr^{sc} with a Leu at Met1 (M1L mutant) by using the QuickChange site-directed mutagenesis kit (Stratagene, Agilent, Madrid, Spain), with specifically designed oligonucleotides. The mutant was verified by automated DNA sequencing (Sistemas Genómicos SL, Valencia, Spain). On this plasmid (M1L), we introduced the mutation M48L, by using the same site-directed mutagenesis kit, with the properly designed oligonucleotides. The corresponding plasmid was introduced into C41 *E. coli* strain [36] and the cells were grown in LB broth. The M1L/M48L was our pseudo-wild-type HPr^{sc}, and it contains the 93 residues of the intact protein On this double-mutant plasmid we introduced each of the mutations to yield the three different mutants: A38M, G58M, G70M.

Expression and purification of M1L/M48L HPr^{sc} was carried out as those of wild-type and the other mutants previously described [30,33]; the yield was similar to that of wild-type protein [30]. The same happened for mutants M1L/A38M/M48L and M1L/M48L/G58M; conversely, the expression of M1L/M48L/G70M was substantially decreased when compared to that of the wild-type protein. Removal of His_6-tag by specific cleavage with thrombin of pseudo-wild-type, M1L/A38M/M48L, M1L/M48L/G58M and M1L/M48L/G70M mutants was identical to that of M1L mutant [19] or wild-type [30].

Purifications of HPr38, HPr58 fragments were similar to that described for the HPr48 fragment [19,37], by using an AKTA-FPLC (GE Healthcare. Barcelona, Spain) system, with a final purification step to separate the corresponding fragment from the intact HPr^{sc} by using a HiTrap SP HP (GE Healthcare, Barcelona, Spain). On the other hand, HPr70 was obtained with a final purification step by using a HiTrap Q HP (GE Healthcare, Barcelona Spain) to separate it from un-cleaved HPr^{sc}; this protocol is different to that of HPr38, HPr48 and HPr58 because HPr70 has an acidic p*I* (similar to that of the intact HPr). The final yield of pure HPr38 was ~60% (from the initial purified mutant); that of HPr58 was ~20% and that of HPr70 was lower than ~ 10%. Identity and integrity of the fragments was confirmed by mass spectrometry and for HPr70 by SDS-PAGE. Concentration of each fragment was calculated from its sole tryptophan, Trp10, by using the extinction coefficient of model compounds [38].

2.3. Protein expression and purification

The wild-type Rsd vector, with a His-tag, containing the Rsd^{ec} was a kind gift from Prof. Ann Hochschild (Harvard, USA). The protein was expressed in C41 *E. coli* strain [36] and the cells were grown in LB broth. The protein was purified as described [28,39]. EIN^{sc} was expressed and purified as described [13,33–35]. HPrK/P^{bs} was a kind gift from Prof. Anne Galinier (Marseille, France), and it was expressed and purified as described [18].

Protein concentrations were determined in all cases from the absorbance of individual amino acids [38].

2.4. Fluorescence

Rsd^{ec} has two tryptophan and eight tyrosine residues; EIN^{sc} has four tyrosine residues; HPrK/P^{bs} has one tryptophan and five tyrosines; and each of the HPr fragments has Trp10. Fluorescence spectra were collected at 25 °C on a Cary spectrofluorimeter (Agilent, Madrid, Spain), with a Peltier temperature controller. The samples were prepared the day before and left overnight at 5 °C. Before measurements, the samples were incubated for 1 h at 25 °C. A 1-cm path-length quartz cell (Hellma, Kruibeke, Belgium) was used.

In the analyses of the ANS and intrinsic fluorescence spectra, we also calculated the average energy of each fragment spectra, $<\lambda>$, which was defined as $<\lambda>=\sum_1^n I_i/\lambda_i/\sum_1^n I_i$ (where I_i is the fluorescence intensity at a wavelength, λ_i).

2.4.1. Intrinsic fluorescence of tryptophan and tyrosines in the fragments

The slit widths were equal to 5 nm for the excitation and emission lights. Protein samples were excited at 280 and 295 nm. The spectra were recorded between 300 and 400 nm. The signal was acquired for 1 s and the increment of wavelength was set to 1 nm. Appropriate blank corrections were made in all spectra. The concentration of each fragment was 20 μM at pH 7.0 (50 mM, phosphate buffer).

2.4.2. ANS fluorescence in the fragments

For ANS experiments, dye concentration was 200 μM, and that of the fragment was 4 μM at pH 7.0 (50 mM, phosphate buffer). Samples were excited at 370 nm, collecting the spectra between 400 and 600 nm, and the rest of the experimental set-up was the same as above.

2.4.3. Fragment-titrations

For the titration between Rsd^{ec}, EIN^{sc} or HPrK/P^{bs}, and HPr38, HPr58 and HPr70 increasing amounts of the fragment, typically in the range of 0–25 μM, were added to a solution with a fixed concentration of the corresponding protein (5 μM for each of them, but it is given in protomer units for HPrK/P^{bs}) in phosphate buffer (50 mM), pH 7.0. The experimental set-up was that described above. The fluorescence of a blank solution, containing only the corresponding protein, was subtracted for each point. The dissociation constant of the complex, K_d, was calculated by fitting the plot of the observed fluorescence change to Refs. [40,41]:

$$F=F_0+\frac{\Delta F_{max}}{2[\text{Protein}]_T}\left([\text{Protein}]_T+[\text{HPr38/HPr58/HPr70}]_T+K_d\right)-\sqrt{\left(\left([\text{Protein}]_T+[\text{HPr38/HPr58/HPr70}]_T+K_d\right)^2-4[\text{Protein}]_T[\text{HPr38/HPr58/HPr70}]_T\right)} \quad (1)$$

where F is the measured fluorescence at any particular concentration of the corresponding fragment after subtraction of the blank; ΔF_{max} is the maximal change in the fluorescence of the fragment when all of the corresponding protein is forming the complex compared to the fluorescence of isolated protein; F_0 is the fluorescence intensity when no fragment was added; $[Protein]_T$ is the constant, total concentration in every titration of each Rsd^{ec}, EIN^{sc} or $HPrK/P^{bs}$ (5 μM, in protomer units, for the latter); and $[HPr48/HPr58/HPr70]_T$ is that of the corresponding fragment, which was varied during every titration. The K_d was determined by following the fluorescence at selected wavelengths and fitting experimental data to Eq. (1). Every titration of the corresponding fragment with each protein was repeated three times, and the variations among the three repetitions were always less than 10% for the different proteins. At all used concentrations, the fluorescence was corrected by the inner-filter effects [42]. Fitting to the above equation was carried out by using KaleidaGraph (Synergy software, Reading, USA). For the fragment HPr38, we also tried to carry out titrations with 3 μM (in protomer units) of each Rsd^{ec}, EIN^{sc} or $HPrK/P^{bs}$, to see whether we could improve the values obtained from the curves (section 3.7.1), but the signal-to-noise ratios of the spectra under those conditions were very poor.

2.5. Circular dichroism

Spectra were collected on a Jasco J810 spectropolarimeter (Jasco, Tokyo, Japan) fitted with a thermostated cell holder and interfaced with a Peltier unit in a 0.1-cm pathlength cell (Hellma, Kruibeke, Belgium). The instrument was periodically calibrated with (+)10-camphorsulphonic acid. Molar ellipticity, [Θ], was calculated as described [43]. All experiments were acquired at pH 7.0 (50 mM, phosphate).

2.5.1. Far-UV CD spectra of the growing fragments of HPr^{sc}

Experiments in the far-UV region with the growing fragments were carried out with the same polypeptide concentrations in the same buffer used in the intrinsic fluorescence studies. Typically, spectra were acquired at a scan speed of 50 nm/min with a response time of 2 s, a bandwidth of 1 nm, and averaged over six scans at 25 °C. Spectra were corrected by subtracting the baseline in all cases. Baseline samples were those containing only the buffer, and subtraction from the spectra of the sample containing the fragments and/or proteins was carried out by using KaleidaGraph (Synergy software). The samples were prepared the day before and left overnight at 5 °C to allow for equilibration. Samples were equilibrated at 25 °C for 1 h before recording the experiments.

2.5.2. Trifluoroethanol-titrations of HPr38, HPr58 and HPr70

For experiments with the three fragments, HPr38, HPr58 and HPr70, in the presence of trifluoroethanol (TFE), the same set of experimental parameters described in the far-UV CD of the isolated fragments was used, except for the fact that experiments were carried out at 5 °C. Fragment concentration was 15 μM. Co-solvent concentrations were indicated in percentage of volume (%). The helical population of each fragment in aqueous solution was determined assuming a two-state helical ↔ random-coil transition (as suggested by the presence of an isodichroic wavelength in the titrations of each fragment) [44,45].

2.6. NMR spectroscopy

All the NMR experiments were performed at 10 °C on an Avance AMX-500 MHz (11.8 T) (Bruker GmbH, Karlsruhe, Germany) with a TXI-probe and z-gradients, and the software Topspin 1.2. The temperature of the probe was calibrated with methanol [46]. All experiments were acquired in phosphate buffer (50 mM, pH 7.0).

2.6.1. 1D-^{1}H NMR spectra

For HPr38, HPr58 and HPr70, 512 scans were acquired with 32 K acquisition points, at concentrations between 40 and 100 μM. Homonuclear 1D-^{1}H NMR spectra were processed after zero-filling. All spectra were referenced to external TSP, considering the pH-dependence of its signals [46].

2.6.2. 2D-^{1}H NMR spectroscopy of HPr38

Two-dimensional experiments on the fragment HPr38 (at ~1.8 mM) were performed with a spectral width of 7801.69 Hz in each dimension and in phase-sensitive mode by using the time-proportional-phase incrementation technique (TPPI) [47].

Standard ^{1}H NMR experiments, as well as TOCSY (80 ms mixing time), ROESY (mixing time 250 ms) and NOESY experiments (mixing time 250 ms) were performed. Data in TOCSY, ROESY and NOESY experiments were acquired with a data matrix size of 4 K (t_2) × 512 (t_1), with the MLEV17 spin-lock sequence [48] in the TOCSY experiments, and 1 s of relaxation time in all experiments. Typically, 80 scans were acquired per t_1 increment, and the residual water signal was removed by using the WATERGATE sequence [49]. NOESY and ROESY spectra [50,51] were collected with, typically, 128 scans per t_1 increment, with the residual water signal removed by the WATERGATE sequence and relaxation time of 1 s. Data were zero-filled, resolution-enhanced with a square sine-bell window function optimized in each spectrum, baseline-corrected, and processed with the Bruker software. The ^{1}H NMR resonances were assigned by standard sequential assignment processes [52]. The random-coil chemical shift values of H_α protons were obtained from tabulated data for model peptides, corrected by neighboring residue effects [53].

We could not carry out the assignments of HPr58 and HPr70 resonances due to: (i) their larger size when compared to that of HPr38 (which hampers the use of only homonuclear experiments); and (ii) the poor final yield of both fragments (which makes impracticable the use of labelling with ^{15}N, as we have previously done with HPr48 [19]).

2.6.3. Translational diffusion NMR (DOSY)of HPr38, HPr58 and HPr70

Fragment concentrations were the same used in the 1D-^{1}H NMR spectra. Translational self-diffusion measurements were performed with the pulsed-gradient spin-echo sequence in the presence of 100% D_2O. The following relationship exists between the translational self-diffusion coefficient, D, and the delays used during experiment acquisition [54]:

$$I/I_0 = -\exp\left(D\gamma_H^2\delta^2G^2(\Delta - \delta/3 - \tau/2)\right) \quad (2)$$

where I is the peak intensity of methyl resonances (in our case) at any gradient strength; I_0 is the maximum peak intensity of the same resonance(s) at the smallest gradient strength (in the three fragments, at 2% of the total power of the gradient coil); D is the translational self-diffusion constant (in $cm^2\ s^{-1}$); δ is the duration (in our case 2.25 ms) of the gradient; G is the gradient strength (in $T\ cm^{-1}$, which was varied in our case between 2 and 95% of the total power of the gradient coil of the probe for each fragment); Δ is the time (for each fragment, 200 ms) between the gradients; γ_H is the gyromagnetic constant of the proton (in $rad\ s^{-1}\ T^{-1}$); and, τ is the recovery delay between the bipolar gradients (100 μs in our experiments for each fragment). The gradient strength was calibrated by using the value of D for the residual proton water line in a sample containing 100% D_2O, placed in a 5-mm tube [54]. Data were plotted as I/I_0 *versus* G^2, and the exponential factor of the curve is $D\gamma_H^2\delta^2(\Delta - \delta/3 - \tau/2)$, from where D can be obtained. A final concentration of 1% of dioxane was added to each fragment; the hydrodynamic radius, R_h, of each polypeptide was obtained for comparison by assuming that the R_h of dioxane was 2.12 Å [55], and the Stokes-Einstein relationship. The DOSY experiment was repeated twice with fresh samples for each fragment.

2.7. Size exclusion chromatography (SEC)

This technique was used to determine the compactness of all fragments [56–58], at concentrations of ~20 μM. Samples were loaded in

50 mM of phosphate buffer (pH 7.0), 150 mM NaCl (to avoid interactions with the column) and 2 mM EDTA (to avoid polypeptide degradation) in a calibrated analytical Superdex 75 10/30 HR FPLC column (GE Healthcare) connected to an AKTA-FPLC (GE Healthcare) at 20 °C. The exclusion molecular weight of the column was 70 kDa for a globular protein, according to the manufacturer. For all fragments, the elution volumes, V_e, were obtained from chromatogram analyses with the UNICORN software (GE Healthcare) from three independent measurements with fresh samples. Samples were eluted at 1 mL/min and continuously monitored with an on-line detector at a wavelength of 280 nm. They were loaded from ice, keeping the minimum delay possible before the injection. The standards used, at 20 μM of protein concentration, for column calibration were: ribonuclease A, chymotrypsinogen A, ovoalbumin and bovine serum albumin. Their elution volumes were measured in the same buffer used for the fragments.

2.8. Biolayer interferometry (BLI)

2.8.1. Experimental design

The association (k_{on}) and dissociation (k_{off}) rate constants of the binding of EIN^{sc}, Rsd^{ec} or $HPrK/P^{bs}$ to HPr38, HPr59 and HPr70 were determined by using a BLItz system (ForteBio, Pall, Barcelona, Spain) [59,60]. The experimental buffer was that recommended by the manufacturer. Since all the proteins had a His-tag, they were immobilized on His-tag biosensors (Forte Bio) at 0.5 μM. Fragment (without the His-tag) concentrations were in the range from 1 to 6 μM during the association step. The general schemes of the protein-association/dissociation reactions for the fragments were: 30 s of initial baseline with the 1 × kinetics buffer (provided by the manufacturer); 120 s of loading protein (EIN^{sc}, Rsd^{ec} or $HPrK/P^{bs}$) into the biosensor; 30 s of baseline with the 1 × kinetics buffer; 120 s of association of any of the fragments to the pre-loaded biosensor; and 120 s of dissociation of any of the fragments from the pre-loaded biosensor.

2.8.2. Fitting of the sensorgrams

Fittings of the sensorgrams was carried out by using KaleidaGraph (Synergy software) working on a PC. The interferometry response during the association step, $R(t)$ (measured in RU), and the binding rate, $dR(t)/dt$, can be used to evaluate the kinetics of the binding of the HPr-fragment (interaction with the biosensor-bound protein), according to:

$$dR(t)/dt = k_{on} \times [\text{HPr-fragment}] \times (R_{max} - R(t)) - k_{off} \times R(t) \quad (3)$$

where R_{max} is proportional to the total concentration of biosensor-bound protein; and [HPr-fragment] represents the concentration of HPr38, HPr58 or HPr70. In the above equation, the $R(t)$ is given by:

$$R(t) = R_{eq} - R_{eq} \times e^{(-k_{obs} \times (t-180))} \quad (4)$$

where R_{eq} is the steady-state, or equilibrium response obtained at infinite time when $dR(t)/dt = 0$. The number 180 in Eq. (4) corresponds to the time, expressed in seconds, at which the association step between immobilized protein and the fragment in the solution starts, in our experimental set-up. Under our conditions for each HPr-fragment and any of the three proteins, we fitted the $R(t)$ as:

$$R(t) = R_{eq} - R_{eq} \times e^{(-k_{obs} \times (t-180))} - R^*_{eq}\ (t - 180) \quad (5)$$

due to slope shown by the RU curve at long times (given by R^*_{eq}). The value of k_{obs} is given by:

$$k_{obs} = k_{on} \times [\text{HPr-fragment}] + k_{off} \quad (6)$$

The dissociation process was always fitted to a single exponential, with $R(t)$ given by:

$$R(t) = R_1 \times e^{(-k_{obs} \times (t-300))} - R_2\ (t - 300) \quad (7)$$

where the indicated figure comes from the time where dissociation of the HPr-fragment from the biosensor-bound protein starts in our experimental set-up, and R_1 is the response level when dissociation starts at 300 s. As for the association step, the last term of Eq. (7) considers the slope of the RU curves at long dissociation times.

3. Results

3.1. Fragment generation

A family of five peptide and fragments of HPr^{sc} was created by using chemical synthesis for the small peptide, HPr^{9-30}, and fragmentation (chemical cleavage) of the full-length protein for the larger peptides (Fig. 1). We introduced methionine residues by protein engineering to be used as cleavage sites for CNBr [45,61]. The sites of mutation were chosen to be at the surface of the protein, or close to that, in a region connecting segments of secondary structure in the native enzyme; thus, positions were chosen to minimize structural changes. In that sense, the fragment HPr^{9-30} comprises the first α-helix and the loop preceding it; HPr38 contains the first and second β-strands and the first α-helix; HPr48, three β-strands and the first α-helix; HPr58, three β-strands and the two first α-helices; and HPr70, the four β-strands and the two first α-helices (Fig. 1). When the fragment HPr^{9-30} was designed, the first β-strand (residues Ala2-Val8, Fig. 1) was excluded to avoid solubility problems, since we were mainly interested in studying the helical propensities of the first α-helix (Ala16-Thr27). All the designed fragments had Trp10, the sole tryptophan in the protein, and then, fluorescence can be used to follow the development of structure in the fragments. The structural features of fragments HPr^{9-30} and HPr48, as monitored by fluorescence, far-UV CD and NMR, have been described before [19,35,37] and they will be described briefly in the sections below to allow for a comparison with the results of the other fragments described in this work.

3.2. Development of the fluorescence of Trp10 on chain elongation as a probe for fragment conformation

Trp10, the sole tryptophan residue, lies deep in one of the cores of the protein, being buried between the first (Ala16-Thr27) and the third (Ala71-Ala83) α-helices. The emission maximum of the fluorescence spectrum of intact HPr^{sc}, described before [30,31], is at ~ 332 nm, probing its correct packing in the native structure of HPr. The steady-state fluorescence spectra of HPr^{9-30} and HPr48 have been described before [19,35,37], showing maxima at ~350 nm, indicating that Trp10 was solvent-exposed (Fig. 2 A). The same behavior can be observed for HPr38, HPr58 and HPr70: all the spectra showed a maximum at ~350 nm. These findings indicate that: (i) in those fragments Trp10 was also solvent-accessible; and, (ii) the tertiary structure around the indole was not native-like. Our results indicate that Trp10 was fully solvent-exposed for all the fragments, but its fluorescence intensity at any wavelength (Fig. 2 B, inset for 350 nm) was smallest in HPr^{9-30} and HPr38, and it grew in HPr48, although it did not acquire a native-like environment until the polypeptide chain was complete (that is, in HPr^{sc} (HPr93)), decreasing in the intensity at 350 nm for the entire chain. The same conclusion can be obtained when the fluorescence intensity at 332 nm is represented *versus* the length of the growing chain, but the graphics is the reverse of that shown in Fig. 2 B, inset, because most of the fragments of the nascent polypeptide chain had a smaller fluorescence intensity at 332 nm. In addition, similar results were obtained by following the $\langle\lambda\rangle$ (Fig. 2 B) *versus* the number of residues in the growing chain (for HPr^{9-30} this value was 30) (Fig. 2 B): the $\langle\lambda\rangle$ was roughly constant until the polypeptide chain was 70-residue long, where it increased to reach a native-like value (2.930 μm^{-1}) The same behavior for the spectral intensity and $\langle\lambda\rangle$ was observed when excitation of Trp10 occurred at 295 nm (Supplementary Material Fig. S1).

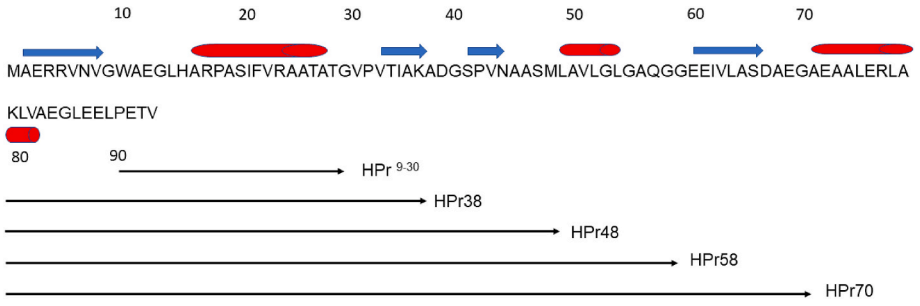

Fig. 1. Sequence of HPr^{sc}. Amino acid sequence and secondary structure of HPr^{sc}, and the positions of cleavage to generate the N-terminal fragments of HPr. The blue arrows indicate β-strands and the red cylinders the α-helices: β-strand1 (Ala2-Val8), α-helix1 (Ala16-Thr27), β-strand2 (Val33-Lys37), β-strand3 (Ser41-Asn44), α-helix2 (Leu49-Leu54), β-strand4 (Glu60-Ser66) and α-helix3 (Ala71-Ala83).

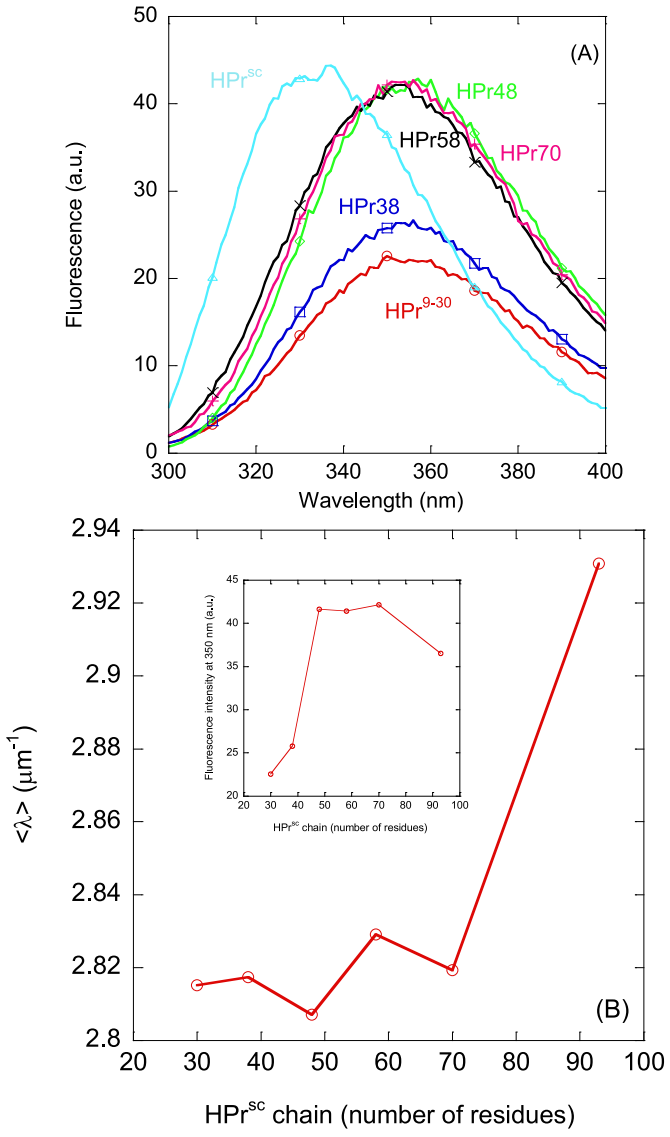

Fig. 2. Fluorescence changes on elongation of the polypeptide chain of HPr^{sc}. (A) Fluorescence spectra of the fragments normalized at 1 μM macromolecule concentration, in phosphate buffer at pH 7.0 (50 mM) and 25 °C. Each spectrum was obtained after excitation at 280 nm. (B) The <λ> of the spectra obtained after excitation at 280 nm *versus* the number of residues in the growing chain. (Inset) The fluorescence intensity at 350 nm after excitation at 280 nm for the growing fragments *versus* the number of residues in the growing chain, in phosphate buffer at pH 7.0 (50 mM) and 25 °C. HPr^{sc} is the pseudo wild-type, 93-residue-long, intact protein.

3.3. Development of the burial of solvent-exposed hydrophobic patches upon chain elongation

A key feature of the structural characterization of the growing chain is the presence of nearby hydrophobic clusters, which become solvent-accessible. As these clusters cannot be detected by any direct spectroscopic probe, we used the binding of the fluorescent dye 8-anilinonaphthalene, 1-sulfonate (ANS). Fluorescence of ANS can be used as a rough index of the accessibility of hydrophobic sites in proteins [62,63].

We explored the capability of all HPr^{sc} fragments to bind ANS, as an indication of the solvent-exposure of hydrophobic patches [64]. If the growing fragments contained solvent-exposed hydrophobic clusters, we should observe that the maximum wavelength of the fluorescence spectra occurred at ~470 nm; by contrast, in the absence of solvent-exposed hydrophobic patches, which are not close enough to bind the probe, the wavelength maximum of fluorescence spectra should be at ~510 nm. None of the fragments showed spectra with maximum wavelength at ~470 nm, indicating that (i) there were not solvent-exposed hydrophobic patches close enough to bind ANS (Fig. 3 A), and; (ii) the regions forming the main hydrophobic core in the intact protein by the first α-helix and the β-sheet were not close enough in the highly dynamic fragments to bind to the probe. The representation of the fluorescence intensity at 510 nm did not present any large variation as the polypeptide chain grew, and only the spectrum of HPr38 showed the largest value of intensity at this wavelength, being the spectrum of HPr70 the second with the larger value (Fig. 3 A). These small variations among the fragments are probably reflecting local conformational changes around several solvent-exposed hydrophobic patches. The representation of the <λ> of the spectra *versus* the number of the amino acids in the growing polypeptide chain presented small variations in the value of <λ> for the different fragments and the whole protein (compare the y-axis scale in Fig. 2 B and 3 B), and probably reflect small, local conformational rearrangements as the polypeptide chain grows (Fig. 3 B), as it happens with the changes in fluorescence intensity at 470 nm.

3.4. Development of secondary structure upon chain elongation measured by far-UV CD

Descriptions of the far-UV CD spectra of HPr$^{9-30}$, HPr48 and the intact HPr^{sc} have been provided elsewhere [19,30,31,35,37]. The far-UV CD spectrum of intact HPr^{sc} [30], similarly to other α/β proteins, is not resolved into contributions from different elements of secondary structure, and it mirrors that of an all-α-helical protein.

The far-UV CD spectra of HPr38, HPr58 and HPr70 were highly similar to that of HPr48 [19]: with an intense minimum at ~ 197 nm and a broad shoulder from 215 to 230 nm (Fig. 4 A). This shape was typical of disordered structures [65–67], where the shoulder at 215–230 nm could be attributed to: (i) the absorbance of aromatic residues (Trp10, His15 and Phe22) and its possible clustering; or (ii) the presence of weak, flickering α-helix-like structures. Deconvolution of the far-UV CD

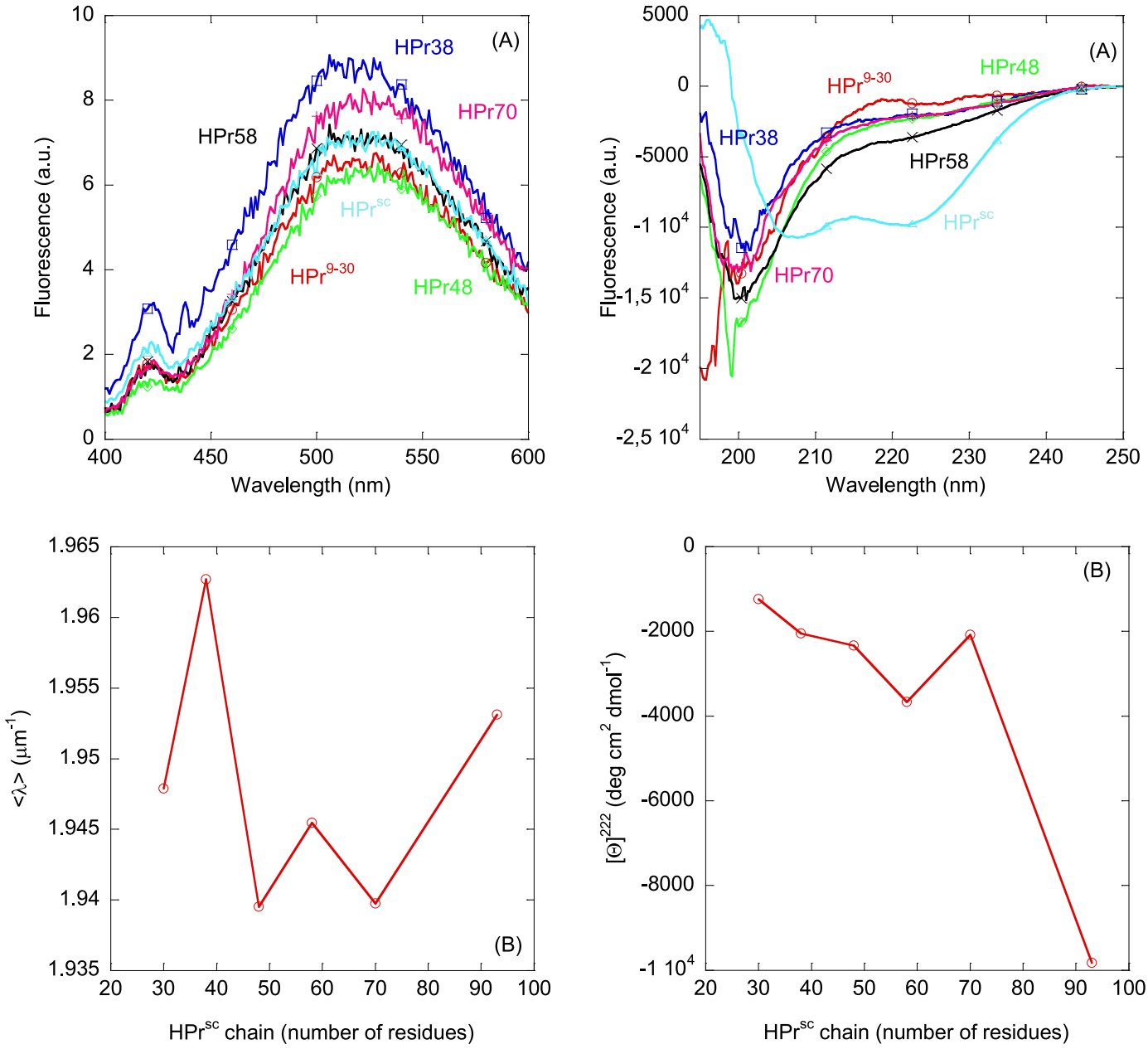

Fig. 3. Solvent-exposure of hydrophobic regions of HPr^{sc} fragments probed by ANS binding. (A) ANS-fluorescence spectra of the fragments normalized at 1 μM macromolecule concentration, in phosphate buffer at pH 7.0 (50 mM) and 25 °C in the presence of 200 μM ANS. (B) The ANS-intensity at 510 nm after excitation at 370 nm for the growing fragments *versus* the number of residues in the growing chain, in phosphate buffer at pH 7.5 (50 mM) and 25 °C. HPr^{sc} is the pseudo wild-type, 93-residue-long, intact protein.

Fig. 4. Secondary structure changes of the growing polypeptide chain of HPr^{sc} probed by far-UV CD. (A) Far-UV CD spectra of the growing fragments of HPr^{sc}, in phosphate buffer at pH 7.0 (50 mM) at 25 °C. (B) The $[\Theta]^{222}$ of the fragments *versus* the number of residues in the growing chain.

spectra of the three fragments by using k2D in the DICHROWEB site [68, 69] indicates that the percentages of helical structures in the fragments were in all cases smaller than 12%. We can further elaborate on the percentages of residual helical structure in the fragments by using two different approaches. First, we can estimate the helical population in the fragments by assuming that a value of −39500 deg cm^2 dmol^{-1} at $[\Theta]^{222}$ is considered 100% of α-helical structure for a polypeptide chain [65–67]. Then, the experimental value of $[\Theta]^{222}$ for HPr38 (−2046 deg cm^2 dmol^{-1}) led to 5% of α-helical structure; that of HPr58 (−3665 deg cm^2 dmol^{-1}) led to 9%; and that of HPr70 (−2077 deg cm^2 dmol^{-1}) led to 5%. These values are similar to those obtained for HPr$^{9-30}$ and HPr48 [19,35,37]. The fact that the helical population among the three fragments was similar, not matter the size, suggests that the residual helical population is confined to the first α-helix (Ala16-Thr27) in the intact HPr^{sc}, because it is the common structural element to all the fragments Although we cannot rule out that those percentages of ordered structure (5%–9%) could involve other elements of the sequence, which are added to the growing chain, the fact that all fragments contain the first α-helix suggests that such region is responsible for that population of folded structure. Furthermore, it is also important to indicate that those values of ellipticity (and then of the helicity) could be affected by the absorbance of aromatic residues at 222 nm [65–67]; in fact, from the HPr^{sc} structure (Fig. 1) the 32% of the secondary structure is helical, but the experimental value of $[\Theta]^{222}$ for HPr^{sc} leads to a 25% of helical structure. Therefore, as a second approach, we tried to estimate the percentages of helical structure in the fragments by using TFE-titrations [44,45,61]. For the three fragments, as it happens in HPr$^{9-30}$ [35,37] and

Table 1
Thermodynamic parameters of the two-state helical ↔ random-coil transition as monitored by TFE titrations at 5 °C for the growing HPr^{sc} fragments.

	m-value (cal/(mol % (v/v))[a]	$[TFE]_{1/2}$ (% (v/v))[a]	ΔG^{water} (kcal/mol)[b]
HPr^{9-30}	166 ± 23[c]	23.2 ± 0.5[c]	3.8 ± 0.5 (0.10%)[c]
HPr38	190 ± 33	19.9 ± 0.7	3.8 ± 0.6 (0.10%)
HPr48	135 ± 41[d]	20 ± 3[d]	2.7 ± 0.9 (0.5%)[d]
HPr58	91 ± 57	30 ± 5	2.7 ± 1.7 (0.5%)
HPr70	187 ± 32	22.8 ± 0.7	4.3 ± 0.8 (0.07%)

[a] Errors in *m*- and $[TFE]_{1/2}$-values were obtained from the fitting of TFE-titration curves to the helical ↔ random-coil transition.
[b] Calculated from the product of the *m*- and $[TFE]_{1/2}$-values. Uncertainties in the Gibbs energy (of helical formation) were obtained from error propagation. The values within the parenthesis indicate the percentage of helical population, assuming a two-state conformational equilibrium [44,45].
[c] Data from Refs. [35,37].
[d] Data from Ref. [37].

HPr48 [37], the TFE-titrations were two state (helical ↔ random-coil) with a single isodichroic point at ~ 203 nm. The TFE-titration measures the differences in ellipticity as the co-solvent concentration was increased at a particular wavelength, and therefore, the detection of the folded population should not be affected by the presence of aromatic residues, if the conformation is the same in the absence or in the presence of the co-solvent. For all the fragments, the *m*- and TFE-values were similar, within the error, and then, the free energy of folding (Table 1). These results further confirm that the helical population in aqueous solution was nearly the same in all the fragments. The populations of helical conformations determined by this method were much smaller than those determined by deconvolution programs or from the value of the $[\Theta]^{222}$ (Table 1).

Therefore, our findings from far-UV CD indicate that HPr38, HPr58 and HPr70 did not show evidence of a well-folded secondary structure, but rather a weak, flickering, native, α-helix-like population seemed to be present in the first α-helix of the protein.

Next, we focused on the recovery of the far-UV CD native spectrum of intact HPr^{sc} during chain elongation, by plotting the $[\Theta]^{222}$ *versus* the number of residues of the growing chain. The $[\Theta]^{222}$ decreased gradually as the polypeptide chain was growing (Fig. 4 B), being smaller (~– 1200 deg cm^2 dmol^{-1}) for HPr^{9-30} to reach the largest value (in absolute number) for the intact protein (~– 9800 deg cm^2 dmol^{-1}). These findings confirm that, as it happens with the tertiary structure around Trp10 monitored by fluorescence (Fig. 2), the native-like secondary structure in HPr^{sc} was only acquired at the latest steps of the growing polypeptide chain.

Table 2
Hydrodynamic measurements for the growing polypeptide chain of HPr[a].

	$D \times 10^{-6}$ (cm^2 s^{-1})	R_h (Å)[b]
HPr^{9-30}	1.95 ± 0.03[c]	11 ± 1 (12.9)
HPr38	1.24 ± 0.08	10 ± 2 (17.4)
HPr48	1.13 ± 0.06[d]	10.9 ± 0.8 (19)
HPr58	0.9 ± 0.2	14 ± 2 (20.5)
HPr70	0.79 ± 0.09	15 ± 2 (23.03)
HPr93 (HPr^{sc})	0.98 ± 0.02[e]	13 ± 2[f]

[a] Errors in the *D* are from the fitting to Eq. (2). All the measurements with the fragments were carried out at 10 °C.
[b] The R_h values of the fragments were obtained from comparison with the R_h of dioxane (2.12 Å) [55]. The value within the parenthesis was calculated from the scale law for disordered polypeptide chains: $R_h = (0.027 \pm 0.01)\ MW^{(0.50 \pm 0.01)}$ [70].
[c] Data from Refs. [35,37].
[d] Data from Ref. [37].
[e] Data from Ref. [96] at pH 6.8 and 20 °C.
[f] Obtained from the comparison with the R_h of dioxane (2.12 Å) and taking into account that the average value of the *D* of dioxane in our DOSY measurements with the different fragments was (6.1 ± 0.4) × 10^{-6} cm^2 s^{-1}.

3.5. Development of biophysical features followed by NMR

3.5.1. Development of the hydrodynamic radius in the growing polypeptide chain

We have previously shown that both HPr^{9-30} [35,37] and HPr48 [19,37] are monomeric, based on the values of the diffusion translation coefficient, *D*. We measured the *D* of HPr38, HPr58 and HPr70, and we compared their values with those of the other fragments and that of the intact protein (Table 2). We could observe that there was a nice gradation in the measured *D* for the different fragments: as the length of the disordered fragment increased, the *D* became smaller, as expected. However, in all fragments, the theoretically calculated R_h value for random-coil polypeptides [70] was larger than that obtained for each fragment from comparison with the experimentally measured *D* of dioxane, assuming the Stokes-Einstein equation (Table 2). These findings suggest that either: (i) the approach of considering the fragments as spheres is not appropriate, since they are disordered (see 3.5.2 and Figs. 2, 4 and 5); or, alternatively, (ii) local contacts tend to make the corresponding fragment more compact around some residues, and for instance, cluster formation around proline residues have been observed in other fragments [71].

3.5.2. Development of secondary and tertiary structures of the growing fragments from NMR

The 1D-^{1}H NMR and 2D-^{1}H NMR spectra of HPr^{9-30} and HPr48 have been described elsewhere [19,35,37] and they indicate that these fragments are disordered (in agreement with the fluorescence and far-UV CD spectra), with the indole signal of Trp10 appearing at 10.20 ppm, as expected in fully solvent-exposed environments [52]. The same can be observed in the 1D-^{1}H NMR spectra of HPr38 and HPr58 (Fig. 5 and Fig. S2), where all the amide (between 8.00 and 8.60 ppm) and the methyl signals (between 0.80 and 1.00 ppm) were clustered at regions where the resonances of random-coil residues are observed, and the indole signal of Trp10 also appeared at ~ 10.20 ppm in both fragments; this value is different to that in a native-like environment of Trp10 in the intact HPr^{sc}, at 9.80 ppm (Fig. 5). It is interesting to note that the signals of the spectrum of HPr58 (Fig. 5 and Fig. S2) were broader than those of the shorter fragments (HPr^{9-30}, HPr38 and HPr48) suggesting some conformational exchange within the NMR time scale. It could be thought that as HPr48 has a tendency to aggregate at the NMR concentrations used for the 2D- and 3D- NMR experiments [19], the same was happening in HPr58, however, at this point we can rule out fragment aggregation at these concentrations because of the value of the *D* (Table 2). A similar broadening was observed in the 1D-^{1}H NMR spectrum of HPr70 (Fig. 5 and Fig. S2); HPr70 was disordered, as judged from the fluorescence (Fig. 2) and far-UV CD (Fig. 4) results, but the signal corresponding to the sole indole did not appear either at 10.20 (random-coil value) or 9.80 ppm (HPr^{sc}-like value), but rather it showed two broad signals at 10.07 and 10.41 ppm (Fig. 6 A). These results suggest that the aromatic chain in this fragment is affected by a slow-to-medium conformational exchange within the NMR-time scale, where the two environments explored by the indole were not native-like. Thus, this fragment must explore some folded conformations part of the time, and probably, HPr58 was also sampling folded conformations, as suggested by the NMR signal broadening, but the environment around Trp10 was more unfolded than that of the same indole in HPr70.

We further explored the conformations of HPr38 by using 2D-^{1}H NMR experiments, as the expression of its parental mutant was good enough and the cleavage reaction proceeded very well. The assignments of the resonances indicated that the chemical shifts of the H_α protons were similar, for the common residues, to those of HPr^{9-30} and HPr48 (Table ST1); furthermore, the conformational shifts (that is, the

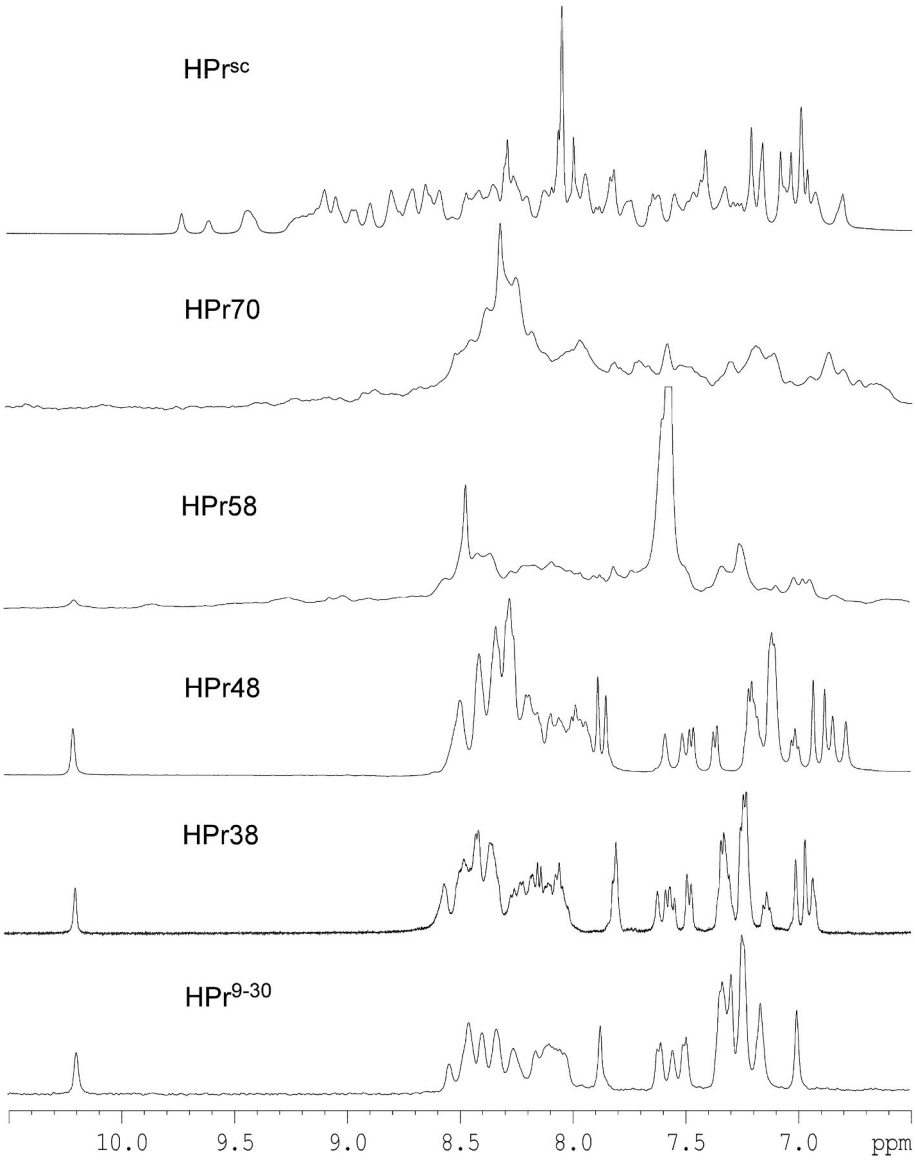

Fig. 5. Secondary and tertiary structure changes in the growing fragments probed by NMR. Down-field (amide) regions of the 1D-^{1}H NMR spectra of the growing chain. The HPr^{sc} is the pseudo wild-type, 93-residue-long protein. Experiments were acquired at 10 °C and pH 7.0 (50 mM, phosphate buffer).

difference between the chemical shift of H_{α} protons of the residues of HPr38 and that of the same residue in a random-coil environment) were similar to those of HPr$^{9\text{-}30}$ for the common regions (Table ST1 and Fig. 4 in Ref. [37]). These similarities further confirm that the fragment (in agreement with CD far-UV and fluorescence results, Figs. 2 and 4) was mainly disordered with evidence of flickering, native-like helical structure around His15.

Therefore, we conclude that the fragments were monomeric and that they did not acquire a native-like secondary and tertiary structures until most of the growing chain was present.

3.6. Variation in the hydrodynamic volume (compactness) of the HPr fragments from SEC

The compactness of the fragments was not only measured by the calculation of the *D*, assuming a spherical shape, but also by SEC. The full-length HPr^{sc} had an elution volume of 12.58 ± 0.06 mL, and we observed a nice increase in the elution volume as the size of the growing chain decreased, going from 17.82 ± 0.02 mL, for HPr$^{9\text{-}30}$, to 13.92 ± 0.05 for HPr70 (Fig. 6 B). That gradual decrease, as the polypeptide chain increased, indicates that the elution of the fragments from the column was mainly dominated by their size. In Fig. S3, the calibration curve obtained for the analytical column used, from the globular proteins, is shown.

All in all, these results confirm that the compactness of the growing polypeptide chain was not native for any of the fragments explored, and then, they were disordered (in agreement with the other biophysical techniques).

3.7. Fragments HPr38, HPr58 and HPr70 were capable of binding to EIN^{sc}, Rsd^{ec} and HPrK/P^{bs}

We have shown above that the presence of residual helical structure in HPr38, HPr58 and HPr70 was flickering around the first α-helix (Ala16-Thr27) of the intact protein, but we wondered if such small population could be responsible for the binding to any of the proteins the intact HPr^{sc} binds to Refs. [28,32,34,35]. In the intact HPr^{sc}, the binding of the three proteins occurs mainly through the first α-helix. We have previously shown that HPr$^{9\text{-}30}$ and HPr48 were capable of binding to those proteins [19,28,34,35], and that in HPr48, residues belonging to

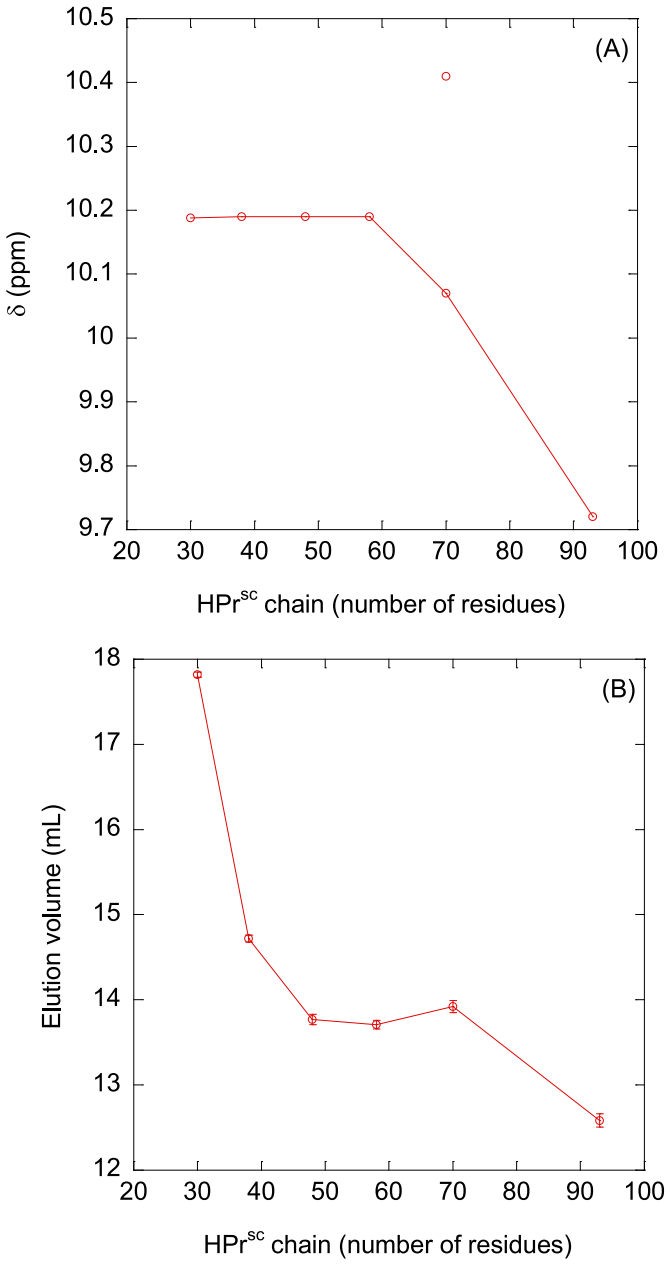

Fig. 6. Other biophysical properties of the growing polypeptide chain. (A) Chemical shift of the indole moiety of Trp10 in the nascent polypeptide chain. For HPr70 the two values of the indole proton are shown. (B) The elution volumes of the growing chain of HPr^{sc} by SEC. The errors are the standard deviations from three different measurements.

the first α-helix (in the intact protein) were affected [19]. We used fluorescence spectroscopy and BLI to determine the affinity constant between each fragment and each of the proteins.

Titration fluorescence measurements have been carried out previously between HPr^{9-30} and EIN^{sc} [34,35] and Rsd^{ec} [28,35]; furthermore, fluorescence or isothermal titration calorimetry (ITC) measurements [33,34] have been also carried out between M1L HPr^{sc} and Rsd^{ec}, or between wild-type HPr^{sc} and EIN^{sc} (Table 3). BLI experiments have been carried out between M1L HPr^{sc}, HPr48 and the three proteins [19]. No BLI experiments could be carried out between HPr^{9-30} and any of the three proteins, due to its small size (as according to manufacturer instructions: binding can be only detected when the macromolecule in the solution, in our case HPr^{9-30}, has a molecular weight higher than 3 kDa).

Table 3
Equilibrium dissociation constant (K_d in μM) of the binding of the nascent chain as measured by several techniques[a].

	EIN^{sc}	Rsd^{ec}	$HPrK/P^{bs}$
HPr^{9-30}	10 ± 7[b], **2.3 ± 0.4**[b]	5 ± 2[b], **2.5 ± 0.4**[c]	-[g]
HPr38	5 ± 2; *1.5 ± 0.6*	*5.8 ± 0.8*	3 ± 2; *1.3 ± 0.4*
HPr48	3.5 ± 0.5[d], *0.3 ± 0.1*[d]	7 ± 3[d], *0.8 ± 0.2*[d]	2 ± 1[d], *0.4 ± 0.1*[d]
HPr58	*1.8 ± 0.3*	*1.6 ± 0.2*	*1.0 ± 0.4*
HPr70	*0.9 ± 0.2*	*7.2 ± 0.6*	*1.2 ± 0.4*
HPr93 (HPr^{sc})	*0.5 ± 0.2*[d], **12 ± 2**[e]	0.2 ± 0.1[f], *1.5 ± 0.8*[d], **2 ± 0.4**[f]	*0.3 ± 0.1*[d]

[a] The values reported were obtained by fluorescence, *BLI* or **isothermal titration calorimetry (ITC)**. The K_d values from kinetic measurements were determined from the rate k_{off}/k_{on} (assuming a two-state binding reaction). Errors in the reported values were obtained from propagation errors in the values of k_{off} and k_{on} obtained from the pseudo-first order plots.
[b] Data from Ref. [34].
[c] Data from Ref. [28]. In Ref. [35] a similar value of 1.4 ± 0.3 μM for the K_d was also measured by ITC.
[d] Data from Ref. [19]. The values for HPr^{sc} were determined by using the M1L HPr^{sc} mutant.
[e] Data from Ref. [34], measured by ITC with wild-type HPr^{sc}.
[f] Taken from Ref. [28], measured with wild-type HPr^{sc}.
[g] Titration fluorescence experiments were carried out in this work to determine an affinity constant of HPr^{9-30}, but although a decrease in fluorescence intensity was observed, such tendency could not be fitted to Eq. (1). Thus, the behavior was similar to that shown in Figs. S4 and S5.

3.7.1. Measuring the binding of HPr38, HPr58 and HPr70 to EIN^{sc}, Rsd^{ec} and $HPrK/P^{bs}$ by fluorescence

We tried to determine the binding of each of the three fragments with each of the three proteins. In all cases (Figs. S4 and S5), we observed a decrease in the fluorescence intensity (when compared to the addition spectrum obtained by the sum of the spectra of the fragment and the molecule), but in all cases, except for HPr38 (Fig. 7), we could not fit such variations to Eq. (1). These findings suggest that the dissociation constants of the binding reaction of HPr58 and HPr70 for each of the three proteins, as determined by fluorescence, were smaller than the fixed concentration of protein used in the experiments (5 μM, although we tried a lower concentration of the three proteins (3 μM) with HPr38, we could not obtain any reliable value of the dissociation constant due to the poor signal-to-noise ratio during the titrations). In HPr38 for EIN^{sc} and $HPrK/P^{bs}$, the constants were 5 ± 2 μM and 3 ± 2 μM, respectively (Fig. 7, Table 3); but we could not obtain a reliable fitting for the Rsd^{ec} titration with HPr38 (data not shown).

3.7.2. Measuring the binding of HPr38, HPr58 and HPr70 to EIN^{sc}, Rsd^{ec} and $HPrK/P^{bs}$ by BLI

As the fluorescence measurements did not yield quantitative values for the dissociation constants of HPr58 and HPr70 for the proteins, probably due to the small value of such constants, we used BLI. With this technique, we could measure all the K_d values for the three fragments for every protein (Table 3), obtained from pseudo-first order plots (Fig. 8, Fig. S6).

The values from BLI, assuming a two-state binding reaction for the formation of the corresponding complex (fragment/protein), were within the same order of magnitude among all the fragments and proteins, ranging from 0.3 to 7 μM (Table 3). In general terms, it seems that the K_d values for EIN^{sc} and $HPrK/P^{bs}$ in all fragments, as measured by BLI, were similar and smaller than those of Rsd^{ec}, but for HPr48 and HPr58, the K_d values among the three proteins were similar within the error. We cannot rationalize easily the differences observed among the fragments, and we hypothesize they could be due to their different flexibility and size. On the other hand, comparison among the values from BLI measured for HPr^{sc} and each fragment for each of the three

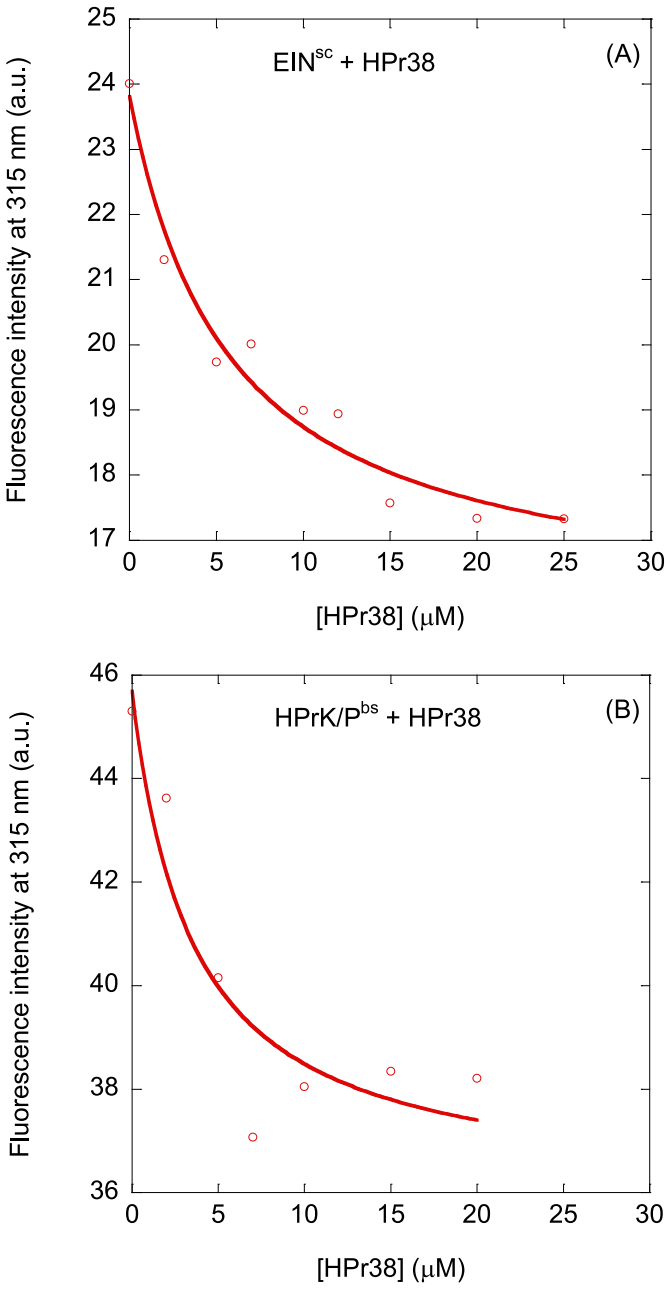

Fig. 7. Binding between HPr38 and the proteins as monitored by fluorescence titrations. (A) Changes in the fluorescence emission at 315 nm of EIN^{sc} with increasing amounts of HPr38 after excitation at 280 nm at 25 °C. (B) Changes in the fluorescence emission at 315 nm of $HPrK/P^{bs}$ with increasing amounts of HPr38, after excitation at 280 nm at 25 °C. The line through the data is the fitting to Eq. (1). Experiments were carried out in 50 mM phosphate buffer (pH 7.0).

proteins, suggests that all the measured values are within the same order of magnitude. However, for the three proteins, HPr48 had the most similar values of the K_d to those of HPr^{sc}. The rest of the fragments, although the K_d values were similar within the error, had slightly larger values than those of HPr^{sc} (Table 3), indicating that the intact protein had a larger affinity for the three proteins, probably because of the presence of a well-folded structure around the binding site (His15).

For HPr38, where the dissociation constants were also measured by fluorescence (Table 3), the measurements obtained were larger than those obtained by BLI. However, it is expected that characterization of binding by using different techniques may yield dissimilar binding

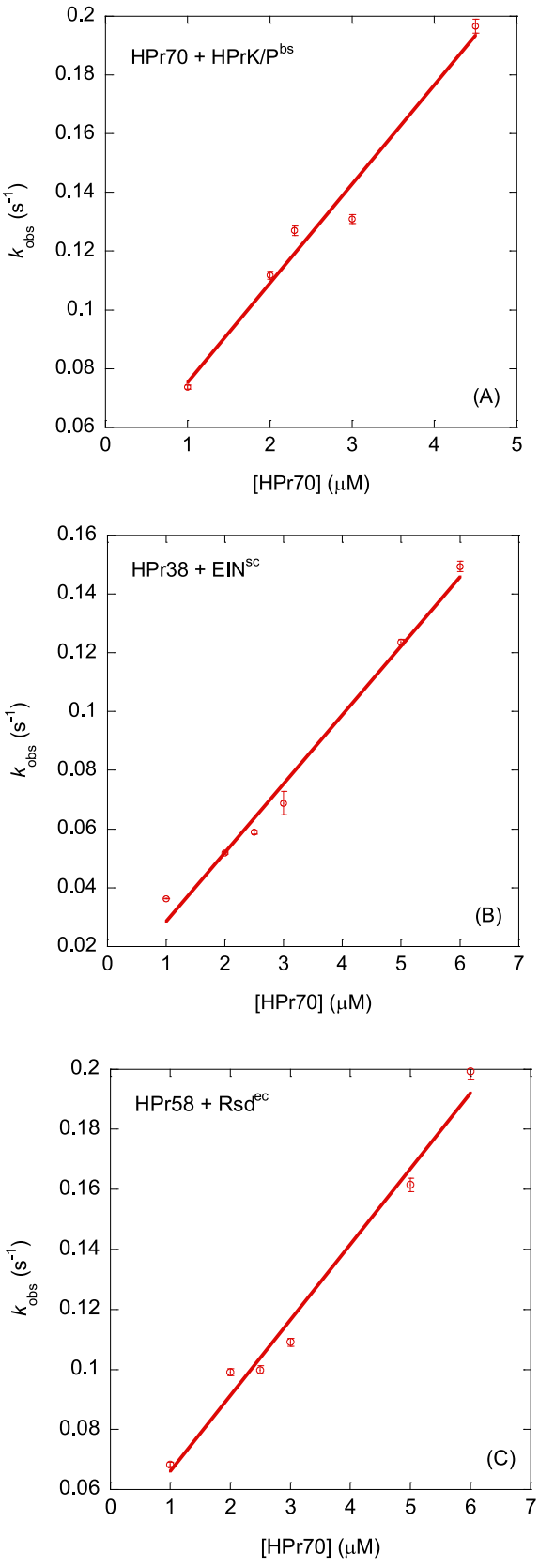

Fig. 8. Kinetics of the binding between an HPr-fragments and the proteins as monitored by BLI. Pseudo-first order plot for the BLI-detected association between selected fragments and some of the proteins. Errors are fitting errors from the fitting of the sensorgrams to Eq. (5).

parameters. Steady-state techniques, where the observable is the equilibrium state (e.g., fluorescence titration), may provide different affinities than transient event ones (such as BLI), where the observable parameters mainly reflect the first encounter between the interacting molecules. In addition, BLI, can provide higher affinity values (and therefore smaller K_d values) because of mass transfer effects on the biosensor-immobilized protein. Furthermore, if the kinetic process has several steps, we should obtain an apparent K_d value, which might not correspond to the real one [59]. Similar discrepancies in the affinities reported by using several techniques, have been observed when measuring interactions in other proteins [19,28,33,72,73].

To sum up, our results suggest that: (i) binding of the growing fragments to each protein is governed by the same element of secondary structure present in all the fragments: the first α-helix; and, (ii) the addition of other elements of secondary structure of the intact HPr^{sc} did not affect the affinity of the fragments for each protein.

4. Discussion

4.1. Interactions in the growing chain of HPr^{sc}

The results from the complementary biophysical techniques indicate that the secondary and tertiary structures in HPr^{sc} are formed in parallel when most of the polypeptide chain is present, that is, when some of the last twenty residues are added. Since: (i) approximately twenty residues are always covered by the ribosome during protein synthesis and bound to tRNA; and (ii) the peptidyl-tRNA is fixed on a ribosome, it is unlikely that HPr^{sc} folds co-translationally as it is synthesized from the ribosome [4,5,74].

Although there is a small population of helical structure around the first α-helix (Ala16-Thr27), it is only the addition of the last long α-helix (Ala71-Ala83) which triggers concomitantly the formation of the tertiary and secondary structures in HPr^{sc}. The remaining elements of secondary structure, namely the second α-helix and most of the four-stranded β-sheet, do not seem to increase the population of helical structure in the first α-helix, and therefore non-native tertiary contacts do not seem to raise. However, there were probably non-native contacts in the growing polypeptide chain among far-away distant residues in the primary structure, as judged by the broadening of signals in the 1D ^{1}H NMR spectra of HPr58 and HPr70 (Fig. 5 and Fig. S2). On the contrary, when the third α-helix of the protein is added to the growing chain, the docking between the first α-helix, the β-sheet and the third α-helix happens (forming the main hydrophobic core of the protein), enhancing the population of native-like, helical structure in the first halve of the protein, making this element acquire a rigid, stable conformation. Long-range interactions of such helix with the second last halve of the protein are key to attain a stable fold.

It is tempting to compare the folding of the growing chain of HPr^{sc} described in this work, with the folding of the intact HPr^{ec}, the HPr from *Escherichia coli*, from an unfolded state originated by the presence of guanidinium hydrochloride (GdmCl). It has been shown that HPr^{ec} folds slowly from GdmCl in a two-state manner, with no intermediates accumulated [75,76], and only the detection of local rearrangements around Phe22 (which is a residue conserved in HPr^{sc}, Fig. 1) is observed [77]. However, at the very early stages of HPr^{ec} folding, a hydrophobic collapse is observed around all phenylalanine residues mainly to bury hydrophobic amino acids, which are close enough in the intact chain [78]. The findings of the growing chain of HPr^{sc} in this work indicate that there was no proximity among the hydrophobic, solvent-exposed patches, as there was not a large increase of the ANS fluorescence as the chain grows (Fig. 3). This apparent discrepancy between the folding of the whole HPr^{ec} and the growing polypeptide could be due to the larger mobility of the fragments because of their smaller size, when compared to that of the intact chain.

4.2. Comparison with the growing polypeptide chains from other proteins

Different strategies have been developed to monitor co-translational folding in real time [79,80]. However, identification and characterization of the different folded states in the growing chain in the ribosome is difficult. An alternative strategy involves the isolation and analysis of translationally arrested polypeptide chains to examine the equilibrium states at a particular co-translational length [81–83]. Equilibrium states of a growing chain can be obtained and studied at equilibrium by designing fragments with the use of protein engineering procedures. In the next paragraphs, we describe briefly what has been found for those other chains and how it compares with the results described in this work:

(a) *The N-terminal growing fragments of CI2*: Shorter fragments do not show evidence of native-like structure except for local clustering around the sole tryptophan of the polypeptide chain [84]. However, the 40-residue-long fragment shows local non-native hydrophobic clusters, with strong binding of ANS [84]; this is probably what happened to fragments HPr58 and HPr70 (Fig. 5), although they do not bind to ANS (Fig. 4). Thus, it seems that there is a minimum size in the growing polypeptide chain, where it starts to explore non-native conformations; for either CI2 or HPr^{sc}, that size seems to be around 60% of the whole polypeptide chain (40 out of 64 in CI2 and 58 out of 93 in HPr^{sc}). The 53- and 60-residue-long fragments of CI2 show native-like secondary structure, but no tertiary one [84,85]. However, in CI2 as in HPr^{sc}, until the growing chain is not 64-residue-long, no compact, native-like structure, with a cooperative unfolding transition, is observed [84,85].

(b) *The N-terminal growing fragments of barnase:* The 110-residue-long barnase was dissected in 7 fragments from its N terminus. The shorter fragments have flickering residual structure around the first, α-helix [86], although they were mainly disordered. A 95-residue-long fragment shows also broadened 1D-^{1}H NMR spectra, and it does not bind ANS (this fragment contains around 85% of the whole chain), but it does not show cooperative unfolding [86]. Only when the growing chain was 105-residue--long, native-like, compact residual structure is observed.

(c) *The C-terminal growing fragments of barnase*: Although a polypeptide chain is not growing from its C terminus during its biological synthesis, barnase chain was dissected to grow from its C-terminal region to compare with the findings from the N-terminal nascent chain. There was evidence of flickering structure around the last β-hairpin (residues Ser92-Leu95) of the protein, with non-native local interactions [87,88]. It is only when the first N-terminal 23-residues are missing when a compact, native-like structure is present. Then, the barnase chain either growing from the N- or the C-terminus follows the same behavior as CI2 and HPr^{sc}: only until the growing chain has most of the residues does not acquire a native-like fold.

(d) *The overlapping dihydrofolate reductase (DHFR) fragments*: Eight overlapping fragments of the 187-residue-long DHFR were designed to dissect the autonomous folding units of this protein [89]. Fragment 37–159 has significant secondary and tertiary structures, with a native-like fold and it unfolds cooperatively in a two-state manner. These findings mean that until the growing chain does not contain around 85% of the whole polypeptide, as it happens with the N-terminal growing chain of barnase, it does not acquire a well-folded structure.

These results and ours in this work do not agree with recent theoretical findings. It has been suggested that folding of a nascent polypeptide chain, especially the formation of α-helices, could start at the distal region of the PET and continue at the depression close to the exit site [90]. Furthermore, it has been observed that multi-immunoglobulin-like-domain proteins can stabilize some partially

folded intermediates, during biosynthesis [91], and even in large proteins, whose folding is under kinetic control, intermediates can be observed during release from the PET [92]. However, all those intermediates have spectroscopic features of molten-globules [93], with broadened 1D-^{1}H NMR spectra, and probably, they do not unfold co-operatively. It is interesting to pinpoint at this stage that larger fragments of CI2 also have molten-globule like features [84,85].

To sum up, the results in this work with HPr^{sc}, and previous findings with different growing chains at equilibrium, indicate that until most of the polypeptide chain is not present, the protein does not acquire a well-formed, stable core with a co-operative unfolding.

4.3. Binding versus folding of growing polypeptide chains

Although there is no evidence of a well-folded, stable structure in any of the HPr^{sc} fragments, they were bound to EIN^{sc}, Rsd^{ec} and HPrK/P^{sc} (Figs. 7 and 8, Figs. S4 and S5). We have tested the binding of HPr$^{9\text{-}30}$ and HPr48 to those proteins [19,32–35], by using fluorescence, CD, ITC, BLI and NMR (in this latter case by using STD-NMR of HPr$^{9\text{-}30}$ and 2D-^{15}N,^{1}H-HSQC spectra of HPr48). The interacting region in both fragments involves residues around His15, the binding site of the protein [19,32], as it happens in the intact polypeptide (Table 3). Furthermore, this region is also involved in the binding of intact HPr to: (i) EIN [17]; (ii) intact Rsd^{ec} [26,27]; and (iii) fragments of Rsd^{ec} comprising some of its helices [28].

In this work we have tested, by using BLI (and for HPr38 by fluorescence, as well), that the binding of HPr38, HPr58 and HPr70 with each of the three proteins also occurred, and then, it is safe to assume that binding also involved the region around His15. This region has a short population of flickering, native-like α-helix [37]. That is, even a small population of helical, native-like structure around the binding site of the entire protein can ensure binding to the natural partners of the intact protein. Thus, it is not necessary to have a well-folded structure to achieve the binding, and, most importantly, the affinity of the fragment for each protein was similar to that of the intact protein (Table 3). This finding is important since one of the fundamental problems in detecting co-translational folding is the ability of using experimental strategies detecting native-like structure. Use of antibodies haven been recognized, for a long time, as a proper tool to detect protein conformation on the ribosome [93–95], and we believe, that in those examples, the antibodies were also monitoring flickering native-like structure, as that detected in this work for the three partner proteins around the binding site of HPr^{sc}.

5. Conclusion

To conclude, we have shown that in HPr^{sc} there is no evidence of well-formed, native-like secondary and tertiary structures, until the growing chain does not contain most of the 93-residue long polypeptide chain. Only native-like, secondary structure, which was not stabilized by the addition of other secondary structure elements as the polypeptide chain grows, was observed at the first α-helix in a small population. The growth of structure in the nascent polypeptide chain of HPr^{sc} was highly co-operative and it did not result from the hierarchical accretion of residual, well-formed secondary structures at each of the different elongating steps. The flickering secondary structure at the first α-helix was recognized by the natural protein partners of the intact polypeptide chain.

6. Supporting information available

One table containing the assignment of HPr38 (Table ST1). There are six figures: the fluorescence spectra of the growing fragments obtained by excitation at 295 nm (Fig: S1); the methyl region of the 1D-^{1}H NMR spectra for the fragments and pseudo-wild-type HPr^{sc} (Fig. S2); the calibration curve of the analytical gel filtration column used (Fig. S3); the fluorescence titration curves with HPrK/P^{bs} and two selected fragments obtained by excitation at 280 nm (Fig. S4); the fluorescence titration curves with Rsd^{sc} and two selected fragments obtained by excitation at 280 nm (Fig. S5); the sensorgrams from BLI for some of the growing fragments with selected proteins (Fig. S6).

Data availability

The data are available from the corresponding author upon reasonable request.

Funding

This research has been funded by la Consellería de Innovación, Universidades, Ciencia y Sociedad Digital (Generalitat Valenciana, Valencian Regional Government) [CIAICO 2021/0135 to JLN]. Some of the NMR equipment used in this work has been funded by Generalitat Valenciana (Spain) and co-financed with ERDF funds (OP ERDF of Generalitat Valenciana (Spain) 2014–2020). The funders did not have any role during acquisition and analyses of experiments or in the publication of this manuscript.

Declaration of competing interest

Declaration of interest: none.

Acknowledgements

The HPr^{sc} was a kind gift from Dr. F. Titgemeyer (Erlangen, Germany); Rsd^{ec} was a kind gift from A. Hochschild (Harvard, USA); and HPrK/P^{bs} was a kind gift of Anne Galinier (Marseille, France). We thank the two anonymous reviewers for helpful suggestions and discussions.

Appendix A. Supplementary data

Supplementary data to this article can be found online at https://doi.org/10.1016/j.abb.2023.109538.

References

[1] D. Balchin, M. Hayer-Hartl, F.U. Hartl, *In vivo* aspects of protein folding and quality control, Science 353 (2016) aac4354, https://doi.org/10.1126/science.aac4354.
[2] R. Rosenzweig, N.B. Nillegoda, M.P. Mayer, B. Bukau, The Hsp70 chaperone network, Nat. Rev. Mol. Cell Biol. 20 (2019) 665–680, https://doi.org/10.1038/s41580-019-0133-3.
[3] S. Preissler, E. Deuerling, Ribosome-associated chaperones as key players in proteostasis, Trends Biochem. Sci. 37 (2012) 274–283, https://doi.org/10.1016/j.tibs.2012.03.002.
[4] G. Kramer, A. Shiber, B. Bukaum, Mechanisms of cotranslational maturation of newly synthesized proteins, Annu. Rev. Biochem. 88 (2019) 337–364, https://doi.org/10.1146/annurev-biochem-013118-111717.
[5] Y. Chen, B. Tsai, N. Li, N. Gao, Structural remodeling of ribosome associated Hsp40-Hsp70 chaperones during co-translational folding, Nat. Commun. 13 (2022) 3410, https://doi.org/10.1038/s41467-022-31127-4.
[6] A. Ishihama, Adaption of gene expression in stationary phase bacteria, Curr. Opin. Genet. Dev. 7 (1997) 582–589, https://doi.org/10.1016/s0959-437x(97)80003-2.
[7] J. Deutscher, The mechanisms of catabolite repression in bacteria, Curr. Opin. Microbiol. 11 (2008) 87–93, https://doi.org/10.1016/j.mib.2008.02.007, doi:.
[8] B. Görke, J. Stülke, Carbon catabolite repression in the bacteria, Nat. Microbiol. 6 (2008) 613–624, https://doi.org/10.1038/nrmicro1932.
[9] J.W. Lengeller, K. Jahreis, Bacterial PEP-dependent carbohydrate: phosphotransferase systems couple sensing and global control mechanisms, Contrib. Microbiol. 16 (2009) 65–87, https://doi.org/10.1159/000219373.
[10] M.G. Gunnewijk, P.T. van den Bogaard, L.M. Veenhoff, E.H. Heuberger, W.M. de Vos, M. Kleerebezem, O.P. Kuipers, B. Poolman, Hierarchical control *versus* autoregulation of carbohydrate utilization in bacteria, J. Mol. Microbiol. Biotechnol. 3 (2001) 401–413.
[11] A. Galinier, J. Deutscher, Sophisticated regulation of transcriptional factors by the bacterial phosphoenolpyruvate: sugar phosphotransferase system, J. Mol. Biol. 429 (2017) 773–783, https://doi.org/10.1016/j.jmb.2017.02.006.
[12] B.R. Lee, P. Lecchi, L. Panell, H. Jaffe, A. Peterkosfsky, Identification of the N-terminal domain of enzyme I of the *Escherichia coli* phosphoenolpyruvate:sugar phosphotransferase system produced by proteolytic digestion, Arch. Biochem. Biophys. 312 (1994) 121–124, https://doi.org/10.1006/abbi.1994.1289.

[13] M. Romero-Beviar, S. Martínez-Rodríguez, J. Prieto, E. Goormaghtigh, U. Ariz, M. de L. Martínez-Chantar, J. Gómez, J.L. Neira, The N-terminal domain of the enzyme I is a monomeric well-folded protein with a low conformational stability and residual structure in the unfolded state, Protein Eng. Des. Sel. 23 (2010) 729–742, https://doi.org/10.1093/protein/gzq045.
[14] E. Hurtado-Gómez, F.N. Barrera, J.L. Neira, Structure and conformational stability of the enzyme I of *Streptomyces coelicolor* explored by FTIR and circular dichroism, Biophys. Chem. 115 (2005) 229–233, https://doi.org/10.1016/j.bpc.2004.12.032.
[15] E. Hurtado-Gómez, G. Fernández-Ballester, H. Nothaft, J. Gómez, F. Titgemeyer, J. L. Neira, Biophysical characterization of the enzyme I of the *Streptomyces coelicolor* phosphoenolpyruvate:sugar phosphotransferase system, Biophys. J. 90 (2006) 4592–4604, https://doi.org/10.1529/biophysj.105.076935.
[16] M. Weigel, M.A. Kukuruzinska, A. Nakazawa, E.B. Waygood, S. Roseman, Sugar transport by the bacterial phosphotransferase system. Phosphoryl transfer reactions catalyzed by enzyme I of *Salmonella typhimurium*, J. Biol. Chem. 257 (1982) 14477–14491.
[17] G.M. Clore, V. Venditti, Structure, dynamics and biophysics of the cytoplasmic protein-protein complexes of the bacterial phosphoenolpyruvate sugar phosphotransferase system, Trends Biochem. Sci. 38 (2013) 515–530, https://doi.org/10.1016/j.tibs.2013.08.003.
[18] J.L. Neira, A. Cámara-Artigas, J.G. Hernández-Cifre, M.G. Ortore, The histidine phosphocarrier Kinase/Phosphorylase from *Bacillus Subtilis* is an oligomer in solution with a high thermal stability, Int. J. Mol. Sci. 22 (2021) 3231, https://doi.org/10.3390/ijms22063231.
[19] J.L. Neira, M. Palomino-Schätzlein, E. Hurtado-Gómez, M.G. Ortore, A. Falcó, An N-terminal half fragment of the histidine phosphocarrier protein, HPr, is disordered but binds to HPr partners and shows antibacterial properties, Biochim. Biophys. Acta Gen. Subj. 1865 (2021), 130015, 1016/j.bbagen.2021.130015.
[20] C.A. Gross, C. Chan, A. Dombroski, T. Gruber, M. Sharp, J. Tupy, B. Young, The functional and regulatory roles of sigma factors in transcription, Cold Spring Harbor Symp. Quant. Biol. 63 (1998) 141–155, https://doi.org/10.1101/sqb.1998.63.141.
[21] E.A. Campbell, O. Muzzin, M. Chlenov, J.L. Sun, C. Anders Olson, O. Weinman, M. L. Trester-Zedlitz, S.A. Darst, Structure of the bacterial RNA polymerase promoter specificity σ factor, Mol. Cell 9 (2002) 527–539, https://doi.org/10.1016/S1097-2765(02)00470-7.
[22] T.M. Gruber, C.A. Gross, Multiple sigma subunits and the portioning of bacterial transcription space, Annu. Rev. Microbiol. 57 (2003) 441–466, https://doi.org/10.1146/annurev.micro.57.030502.090913.
[23] A. Ishihama, Functional modulation of *Escherichia coli* RNA polymerase, Annu. Rev. Microbiol. 54 (2000) 499–518, https://doi.org/10.1016/0065-227x(90)90005-e.
[24] M. Jishage, A. Ishihama, A stationary phase protein in *Escherichia coli* with binding activity to the major sigma subunit of RNA polymerase, Proc. Natl. Acad. Sci. USA 95 (1998) 4953–4958, https://doi.org/10.1073/PNAS.95.9.4953.
[25] M. Jishage, A. Ishihama, Transcriptional organization and *in vivo* role of the *Escherichia coli rsd* gene, encoding the regulator of RNA polymerase sigma D, J. Bacteriol. 181 (1999) 3768–3776, https://doi.org/10.1128/jb.181.12.3768-3776.1999.
[26] Y.H. Park, C.R. Lee, M. Choe, Y.K. Seok, HPr antagonizes the anti-σ^{70} activity of Rsd in *Escherichia coli*, Proc. Natl. Acad. Sci. USA 110 (2013) 21142–21147, https://doi.org/10.1073/pnas.1316629111.
[27] Y.H. Park, S.H. Um, S. Song, Y.J. Seok, N.C. Ha, Structural basis for the sequestration of the anti-σ^{70} factor Rsd from σ^{70} by the histidine-containing phosphocarrier protein HPr, Acta Crystallogr. D Biol. Crystallogr. 71 (2015) 1998–2008, https://doi.org/10.1107/S1399004715013759.
[28] J.L. Neira, F. Hornos, C. Cozza, A. Cámara-Artigas, A. Abián, A. Velázquez-Campoy, The histidine phosphocarrier protein, HPr, binds to the highly thermostable regulator of sigma D protein, Rsd, and its isolated helical fragments, Arch. Biochem. Biophys. 639 (2018) 26–37, https://doi.org/10.1021/acs.biochem.6b00135.
[29] M.S.B. Paget, H.J. Hong, M.J. Bibb, M.J. Buttner, The ECF sigma factors of *Streptomyces coelicolor* A3(2), in: D.A. Hodgson, D. A, C.M. Thomas (Eds.), SGM Symposium 61: Signals, Switches, Regulons and Cascades: Control of Bacterial Gene Expression, Cambridge University Press, Cambridge, 2002, pp. 105–125.
[30] G. Fernández-Ballester, J. Maya, A. Martin, S. Parche, J. Gómez, F. Titgemeyer, J. L. Neira, The histidine-phosphocarrier protein of *Streptomyces coelicolor* folds by a partially folded species at low pH, Eur. J. Biochem. 270 (2003) 2254–2267, https://doi.org/10.1046/J.1432-1033.2003.03594.X.
[31] J.L. Neira, J. Gómez, The conformational stability of the *Streptomyces coelicolor* histidine-phosphocarrier protein. Characterization of cold denaturation and urea-protein interactions, Eur. J. Biochem. 271 (2004) 2165–2181, https://doi.org/10.1111/j.1432-1033.2004.4142.x.
[32] E. Hurtado-Gómez, O. Abián, F.J. Muñoz, M.J. Hernáiz, A. Velázquez-Campoy, J. L. Neira, Defining the epitope region of a peptide from the *Streptomyces coelicolor* phosphoenolpyruvate:sugar phosphotransferase system able to bind to the enzyme I, Biophys. J. 95 (2008) 1336–1348, https://doi.org/10.1529/biophysj.107.126664.
[33] R. Doménech, A.I. Martínez-Gómez, D. Aguado-Llera, S. Martínez-Rodríguez, J. M. Clemente-Jiménez, A. Velázquez-Campoy, J.L. Neira, Stability and binding of the phosphorylated species of the N-terminal domain of enzyme I and the histidine phosphocarrier protein from the *Streptomyces coelicolor* phosphoenolpyruvate: sugar phosphotransferase system, Arch. Biochem. Biophys. 526 (2012) 44–53, https://doi.org/10.1016/j.abb.2012.07.004.
[34] R. Doménech, S. Martínez-Rodríguez, A. Velázquez-Campoy, J.L. Neira, Peptides as inhibitors of the first phosphorylation step of the *Streptomyces coelicolor* phosphoenolpyruvate: sugar phosphotransferase system, Biochemistry 51 (2012) 7393–7402, https://doi.org/10.1021/bi3010494.
[35] J.L. Neira, D. Ortega-Alarcón, B. Rizzuti, M. Palomino-Schätzlein, A. Velázquez-Campoy, A. Falcó, Residual helicity at the active site of the histidine phosphocarrier, HPr, modulates binding affinity to its natural partners, Int. J. Mol. Sci. 22 (2021), 10805, https://doi.org/10.3390/ijms221910805.
[36] B. Miroux, J.E. Walker, Over-production of proteins in *Escherichia coli*: mutant hosts that allow synthesis of some membrane proteins and globular proteins at high levels, J. Mol. Biol. 260 (1996) 289–298, https://doi.org/10.1006/jmbi.1996.0399.
[37] E. Hurtado-Gómez, M. Caprini, J.L. Neira, The helical structure propensity in the first helix of the histidine phosphocarrier protein of *Streptomyces coelicolor*, Protein Pept. Lett. 14 (2007) 281–290, https://doi.org/10.2174/092986607780090784.
[38] S.C. Gill, P.H. von Hippel, Calculation of protein extinction coefficients from amino acid sequence data, Anal. Biochem. 182 (1989) 319–326, https://doi.org/10.1016/0003-2697(89)90602-7.
[39] A.H. Yuan, B.D. Gregory, J.S. Sharp, K. McCleary, S.L. Dove, A. Hochschild, Rsd family proteins make simultaneous interactions with regions 2 and 4 of the primary sigma factor, Mol. Microbiol. 70 (2008) 1136–1151, https://doi.org/10.1111/j.1365-2958.2008.06462.x.
[40] D. Beckett, Measurement and analysis of equilibrium binding titrations: a beginner's guide, Methods Enzymol. 488 (2011) 1–16, https://doi.org/10.1016/B978-0-12-381268-1.00001-X.
[41] C.A. Royer, S.F. Scarlatta, Fluorescence approaches to quantifying biomolecular interactions, Methods Enzymol. 450 (2008) 79–106, https://doi.org/10.1016/S0076-6879(08)03405-8.
[42] B. Birdsall, R.W. King, M.R. Wheeler, C.A. Lewis Jr., S. Goode, R.B. Dunlap, G. C. Roberts, Correction for light absorption in fluorescence studies of protein-ligand interactions, Anal. Biochem. 132 (1983) 353–361, https://doi.org/10.1016/0003-2697(83)90020-9.
[43] J.L. Neira, F. Hornos, J. Bacarizo, A. Cámara-Artigas, J. Gómez, The monomeric species of the regulatory domain of tyrosine hydroxylase has a low conformational stability, Biochemistry 55 (2016) 3418–3431, https://doi.org/10.1021/acs.biochem.6b00135.
[44] A. Jasanoff, A.R. Fersht, Quantitative determination of helical propensities from trifluoroethanol titration curves, Biochemistry 33 (1994) 2129–2135, https://doi.org/10.1021/bi00174a020.
[45] J. Sancho, J.L. Neira, A.R. Fersht, An N-terminal fragment of barnase has residual helical structure similar to that in a refolding intermediate, J. Mol. Biol. 224 (1992) 749–758, https://doi.org/10.1016/0022-2836(92)90559-3.
[46] J. Cavanagh, W.J. Fairbrother, A.G. Palmer, N.J. Skelton, Protein NMR Spectroscopy: Principles and Practice, first ed., Academic Press, New York, 1996.
[47] D. Marion, K. Wüthrich, Application of phase sensitive two-dimensional correlated spectroscopy (COSY) for measurements of 1H-1H spin-spin coupling constants in proteins, Biochem. Biophys. Res. Commun. 11 (1983) 967–974, https://doi.org/10.1016/0006-291x(83)91093-8.
[48] A. Bax, D.G. Davis, MLEV-17-based two-dimensional homonuclear magnetization transfer spectroscopy, J. Magn. Reson. 65 (1985) 355–360, https://doi.org/10.1016/0022-2364(85)90018-6.
[49] M. Piotto, V. Saudek, V. Sklenar, Gradient-tailored excitation for single-quantum NMR spectroscopy of aqueous solutions, J. Biomol. NMR 2 (1992) 661–675.
[50] A. Kumar, R.R. Ernst, K. Wüthrich, A two-dimensional nuclear Overhauser enhancement (2D NOE) experiment for the elucidation of complete proton-proton cross-relaxation networks in biological macromolecules, Biochem. Biophys. Res. Commun. 95 (1980) 1–6, https://doi.org/10.1007/BF02192855.
[51] A. Bax, D.G. Davis, Practical aspects of two-dimensional transverse NOE spectroscopy, J. Magn. Reson. 63 (1985) 207–213, https://doi.org/10.1016/0022-2364(85)90171-4.
[52] K. Wüthrich, NMR of Proteins and Nucleic Acids, John Wiley and Sons, New York, 1986.
[53] S. Schwarzinger, G.J. Kroon, T.R. Foss, J. Chung, P.E. Wright, H.J. Dyson, Sequence-dependent correction of random coil NMR chemical shifts, J. Am. Chem. Soc. 123 (2001) 2970–2978, https://doi.org/10.1021/ja003760i.
[54] A. Czypionka, O.R. de los Paños, M.G. Mateu, F.N. Barrera, E. Hurtado-Gómez, J. Gómez, M. Vidal, J.L. Neira, The isolated C-terminal domain of Ring 1B is a dimer made of stable, well-structured monomers, Biochemistry 46 (2007) 12764–12776, https://doi.org/10.1021/bi701343q.
[55] D.K. Wilkins, S.B. Grimshaw, V. Receveur, C.M. Dobson, J.A. Jones, L.J. Smith, Hydrodynamic radii of native and denatured proteins measured by pulse field gradient NMR techniques, Biochemistry 38 (1999) 16424–16431, https://doi.org/10.1021/bi991765q.
[56] P.J. Darlin, J.M. Holt, G.K. Ackers, Coupled energetics of lambda cro repressor self-assembly and site-specific DNA operator binding I: analysis of cro dimerization from nanomolar to micromolar concentrations, Biochemistry 39 (2000) 11500–11507, https://doi.org/10.1021/bi000935s.
[57] M.I. Muro-Pastor, F.N. Barrera, J.C. Reyes, F.J. Florencio, J.L. Neira, The inactivating factor of glutamine synthetase, IF7, is a "natively unfolded" protein, Protein Sci. 12 (2003) 1443–1454, https://doi.org/10.1110/ps.0303203.
[58] G.K. Ackers, Molecular sieve studies of interacting protein systems. I. Equations for transport of associating systems, J. Biol. Chem. 242 (1967) 3026–3034.
[59] D. Frenzel, D. Willbolds, Kinetic titration series with biolayer interferometry, PLoS One 9 (2014), e106882, https://doi.org/10.1371/journal.pone.0106882.
[60] D. Pantoja-Uceda, J.L. Neira, L. Saelices, R. Robles-Rengel, F.J. Florencio, M. I. Muro-Pastor, J. Santoro, Dissecting the binding between glutamine synthetase and its two natively unfolded protein inhibitors, Biochemistry 55 (2016) 3370–3382, https://doi.org/10.1021/acs.biochem.6b00072.

[61] J. Sancho, A.R. Fersht, Dissection of an enzyme by protein engineering. The N and C-terminal fragments of barnase form a native-like complex with restored enzymic activity, J. Mol. Biol. 224 (1992) 741–747, https://doi.org/10.1016/0022-2836(92)90558-2.
[62] L. Styer, The interaction of a naphthalene dye with apomyoglobin and apohemoglobin, J. Mol. Biol. 13 (1965) 482–495, https://doi.org/10.1016/s0022-2836(65)80111-5.
[63] P.M. Mulqueen, M.J. Kronman, Binding of naphthalene dyes to the N and A conformers of bovine α-lactalbumin, Arch. Biochem. Biophys. 215 (1982) 28–39, https://doi.org/10.1016/0003-9861(82)90275-2.
[64] G.V. Semisotnov, N.A. Rodionova, O.L. Razgulayev, V.N. Uversky, A.F. Gripas, R. I. Gilmanshin, Study of the molten globule intermediate state in protein folding by a hydrophobic fluorescent probe, Biopolymers 31 (1991) 1119–1128, https://doi.org/10.1002/bip.360310111.
[65] R.W. Woody, Circular dichroism, Methods Enzymol. 246 (1995) 34–71, https://doi.org/10.1016/0076-6879(95)46006-3.
[66] S.M. Kelly, T.J. Jess, N.C. Price, How to study proteins by circular dichroism, Biochim. Biophys. Acta, Proteins Proteomics 1751 (2005) 119–139, https://doi.org/10.1016/j.bbapap.2005.06.005.
[67] S.M. Kelly, N.C. Price, The use of circular dichroism in the investigation of protein structure and function, Curr. Protein Pept. Sci. 1 (2000) 349–384, https://doi.org/10.2174/1389203003381315.
[68] L. Whitmore, B.A. Wallace, Protein secondary structure analysis from circular dichroism spectroscopy: methods and reference databases, Biopolymers 89 (2008) 392–400, https://doi.org/10.1002/bip.20853.
[69] L. Whitmore, B.A. Wallace, DICHROWEB, an online server for protein secondary structure analyses from circular dichroism spectroscopic data, Nucleic Acids Res. 32 (2004) W668–W673, https://doi.org/10.1093/nar/gkh371.
[70] J. Danielsson, J. Jarvet, P. Damberg, A. Gräslund, Translational diffusion measured by PFG-NMR on full length and fragments of the Alzheimer Aβ(1-40) peptide. Determination of the hydrodynamic radii of random coil peptide of varying length, Magn. Reson. Chem. 40 (2002) S89–S97, https://doi.org/10.1002/MRC.1132.
[71] J.L. Neira, A. Jiménez-Alesanco, B. Rizzuti, A. Velázquez-Campoy, The nuclear localization sequence of the epigenetic factor RYBP binds to human importin α3, Biochim. Biophys. Acta, Proteins Proteomics 1869 (2021), 140670, https://doi.org/10.1016/j.bbapap.2021.140670.
[72] N. Cremades, A. Velázquez-Campoy, E. Freire, J. Sancho, The flavodoxin from *Helicobacter pylori*: structural determinants of thermostability and FMN cofactor binding, Biochemistry 47 (2008) 627–639, https://doi.org/10.1021/bi701365e.
[73] Y.J. Bollen, A.H. Westphal, S. Lindhoud, W.J. van Berkel, C.P. van Mierlo, Distant residues mediate picomolar binding affinity of a protein cofactor, Nat. Commun. 3 (2012) 1010, https://doi.org/10.1038/ncomms2010.
[74] J. Micic, O. Rodríguez-Galán, R. Babinao, F. Fitzgerald, J. Fernández-Fernández, Y. Zhang, N. Gao, J.L. Woolford, J. de la Cruz, Ribosomal protein eL39 is important for maturation of the nascent polypeptide exit tunnel and proper folding during translation, Nucleic Acids Res. 50 (2022) 6453–6473, https://doi.org/10.1093/nar/gkac366.
[75] N.A.J. Van Nuland, W. Meijberg, J. Warner, W. Forge, R.M. Scheek, G.T. Robillard, C.M. Dobson, Slow cooperative folding of a small globular protein HPr, Biochemistry 37 (1998) 622–637, https://doi.org/10.1021/bi9717946.
[76] A.I. Azuaga, J.L. Neira, N.A.J. Van Nuland, HPr as a model protein in structure, interaction, folding and stability studies, Protein Pept. Lett. 12 (2005) 123–137, https://doi.org/10.2174/0929866053005818.
[77] A.I. Azuaga, D. Canet, G. Smeenk, R. Berends, F. Titgemeijer, R. Duurkens, P. L. Mateo, R.M. Scheek, G.T. Robillard, C.M. Dobson, N.A.J. Van Nuland, Characterization of single-tryptophan mutants of histidine-containing phosphocarrier protein: evidence for local rearrangements during folding from high concentrations of denaturant, Biochemistry 42 (2003) 4883–4895, https://doi.org/10.1021/bi027182p.
[78] D. Canet, C.E. Lyon, R.M. Scheek, G.T. Robillard, C.M. Dobson, P.J. Hore, N.A. J. Van Nuland, Rapid formation of non-native contacts during the folding of HPr revealed by real-time photo-CIDNP NMR and stopped-flow fluorescence experiments, J. Mol. Biol. 330 (2003) 397–407, https://doi.org/10.1016/s0022-2836(03)00507-2.
[79] F. Wruck, A. Katranidis, K.H. Nierhaus, G. Büldt, M. Hegner, Translation and folding of single proteins in real time, Proc. Natl. Acad. Sci. USA 114 (2017) E4399–E4407, https://doi.org/10.1073/pnas.1617873114.
[80] W. Holtkamp, G. Kokic, M. Jäger, J. Mittelstaet, A.A. Komar, M.V. Rodnina, Cotranslational protein folding on the ribosome monitored in real time, Science 350 (2015) 1104–1107, https://doi.org/10.1126/science.aad0344.
[81] A.M.E. Cassaignau, L.D. Cabrita, J. Christodoulou, How does the ribosome fold the proteome? Annu. Rev. Biochem. 89 (2020) 389–415, https://doi.org/10.1146/annurev-biochem-062917-012226.
[82] A.M.E. Cassaignau, H.M. Launay, M.E. Karyadi, X. Wang, C.A. Waudby, A. Deckert, A.L. Robertson, J. Christodoulou, L.D. Cabrita, A strategy for co-translational folding studies of ribosome-bound nascent chain complexes using NMR spectroscopy, Nat. Protoc. 11 (2016) 1492–1507, https://doi.org/10.1038/nprot.2016.101.
[83] L.D. Cabrita, A.M.E. Cassaignau, H.M.M. Launay, C.A. Waudby, T. Wlodarski, C. Camilloni, M.E. Karyadi, A.L. Robertson, X. Wang, A.S. Wentink, L. Goodsell, C. A. Woolhead, M. Vendruscolo, C.M. Dobson, J. Christodoulou, A structural ensemble of a ribosome-nascent chain complex during co-translational protein folding, Nat. Struct. Mol. Biol. 23 (2016) 278–285, https://doi.org/10.1038/nsmb.3182.
[84] G. De Prat Gay, J. Ruiz-Sanz, J.L. Neira, L.S. Itzhaki, A.R. Fersht, Folding of a nascent polypeptide chain *in vitro*: cooperative formation of structure in a protein module, Proc. Natl. Acad. Sci. USA 92 (1995) 3683–3686, https://doi.org/10.1073/pnas.92.9.3683.
[85] G. De Prat Gay, J. Ruiz-Sanz, J.L. Neira, F.J. Corrales, D.E. Otzen, A.G. Ladurner, A. R. Fersht, Conformational pathway of the polypeptide chain of chymotrypsin inhibitors-2 growing from its N terminus *in vitro*. Parallels with the protein folding pathway, J. Mol. Biol. 254 (1995) 968–979, https://doi.org/10.1006/jmbi.1995.0669.
[86] J.L. Neira, A.R. Fersht, Exploring the folding funnel of a polypeptide chain by biophysical studies on protein fragments, J. Mol. Biol. 285 (1999) 1309–1333, https://doi.org/10.1006/jmbi.1998.2249.
[87] J.L. Neira, A.R. Fersht, Acquisition of native-like interactions in C-terminal fragments of barnase, J. Mol. Biol. 287 (1999) 421–432, https://doi.org/10.1006/jmbi.1999.2602.
[88] J.L. Neira, A.R. Fersht, An NMR study of the β-hairpin region of barnase, Folding Des. 1 (1996) 231–241, https://doi.org/10.1016/s1359-0278(96)00034-x.
[89] C.V. Gegg, K.E. Bowers, C.R. Matthews, Probing minimal independent folding units in dihydrofolate reductase by molecular dissection, Protein Sci. 6 (1997) 1885–1892, https://doi.org/10.1002/pro.5560060909.
[90] G. Kramer, V. Ramachandiran, B. Hardesty, Co-translational folding - *omnia mea mecum porto*? Int. J. Biochem. Cell Biol. 33 (2001) 541–553, https://doi.org/10.1016/s1357-2725(01)00044-9.
[91] S.H.S. Chan, T. Włodarski, J.O. Streit, A.M.E. Cassaignau, L.F. Woodburn, M. Ahn, G.J. Freiherr-von Sass, C.A. Waudby, N. Budisa, L.D. Cabrita, J. Christodoulou, The ribosome stabilizes partially-folded intermediates of a nascent multi-domain protein, Nat. Chem. 14 (2022) 1165–1173, https://doi.org/10.1038/s41557-022-01004-0.
[92] E. Plessa, L.P. Chu, S.H.S. Chan, O.L. Thomas, A.M.E. Cassaignau, C.A. Waudby, J. Christodoulou, L.D. Cabrita, Nascent chains can form co-translational folding intermediates that promote post-translational folding outcomes in a disease-causing protein, Nat. Commun. 12 (2021) 6447, https://doi.org/10.1038/s41467-021-26531-1.
[93] B. Friguet, L. Djavadi-Ohaniance, J. King, M.E. Goldberg, *In vitro* and ribosome-bound folding intermediates of P22 tailspike protein detected with monoclonal antibodies, J. Biol. Chem. 269 (1994) 15945–15949.
[94] K. Tokatlidis, B. Friguet, D. Deville-Bonne, F. Baleaux, A.N. Fedorov, A. Navon, L. Djavadi-Ohaniance, M.E. Goldberg, Nascent chains: folding and chaperone interaction during elongation on ribosomes, Philos. Trans. R. Soc. B Biol. Sci. 348 (1995) 89–95, https://doi.org/10.1098/rstb.1995.0049.
[95] A.N. Fedorov, Biosynthetic protein folding and molecular chaperons, Biochemistry (Moscow) 87 (2022) S128–S145, https://doi.org/10.1134/S0006297922140115.
[96] J.A. Poveda, G. Fernández-Ballester, M. Prieto, J.L. Neira, Dynamics of tryptophan in the histidine-containing phosphocarrier protein of *Streptomyces coelicolor*: evidence of multistate equilibrium unfolding, Biochemistry 46 (2007) 7252–7260, https://doi.org/10.1021/bi7002923.